water

MDPI

Supplementary material

Simulation of Heat Flow in a Synthetic Watershed: The Role of the Unsaturated Zone

Eric D. Morway [1,*], Daniel T. Feinstein [2] and Randall J. Hunt [3]

[1] U.S. Geological Survey, Nevada Water Science Center, 2730 N. Deer Run Rd. Suite 3, Carson City, NV 89701, USA
[2] U.S. Geological Survey, Upper Midwest Water Science Center, Milwaukee Office, 3209 North Maryland Avenue, Milwaukee, WI 53211, USA
[3] U.S. Geological Survey, Upper Midwest Water Science Center, 1 Gifford Pinchot Drive, Madison, WI 53726, USA
* Correspondence: emorway@usgs.gov

Supporting Information Section S1–Construction of the model heat forcing function

Monthly spin-up infiltration at the top of the unsaturated zone was set to a constant rate of 8 inches/year (0.203 m/year) for all monthly periods. During the subsequent warming period, the rate varied to reflect seasonal changes and included noise (Figure S1-1); the overall average infiltration rate during the warming period is 8.84 inch/year (0.224 m/year) with no overall trend, but with significant variability within and across years (Table S1-1 and Figure S1-2).

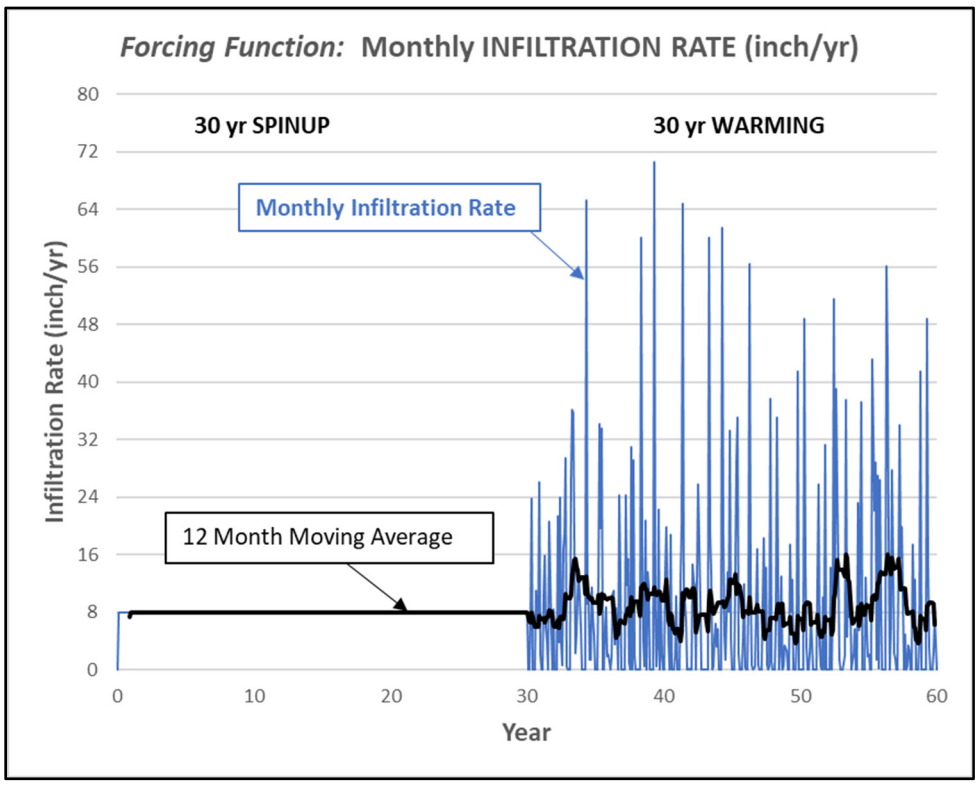

Figure S1-1. Monthly and average yearly infiltration rates over warming period.

INFILTRATION RATES IN INCHES/YEAR

Warming_Year	Jan	Feb	March	April	May	June	July	August	Sept	Oct	Nov	Dec
1	0.000	0.000	7.403	23.716	0.000	0.000	0.000	10.962	6.180	7.293	26.092	1.981
2	0.000	0.000	10.572	15.901	5.873	4.059	0.000	20.587	5.540	0.000	8.433	0.000
3	0.000	0.000	21.341	3.857	23.971	3.603	0.684	16.717	18.917	29.410	0.408	0.000
4	0.000	0.000	26.662	36.190	35.717	18.220	2.288	4.865	10.230	13.925	5.790	0.000
5	0.000	0.000	0.000	65.215	9.121	10.296	1.416	1.416	11.514	7.385	4.738	0.000
6	0.000	0.000	12.781	34.100	19.728	33.477	0.000	0.000	5.996	8.722	1.872	2.152
7	0.000	1.766	10.550	10.949	3.550	8.556	5.488	0.000	24.269	13.947	0.000	0.000
8	0.000	0.000	24.212	11.689	15.340	0.969	0.000	30.913	0.000	29.099	1.845	0.000
9	0.000	0.000	0.000	59.977	17.089	3.971	0.412	20.758	0.000	13.644	11.356	0.000
10	0.000	0.000	0.000	70.527	8.078	0.425	3.515	22.200	0.000	9.257	2.288	0.000
11	0.000	13.508	19.829	3.932	0.000	18.816	0.000	0.000	0.000	2.007	10.155	0.000
12	0.000	0.000	12.509	20.070	64.750	7.661	9.476	6.903	0.000	0.000	0.162	0.000
13	0.000	14.644	12.408	11.602	0.000	25.737	17.905	9.875	0.000	0.000	0.000	0.000
14	0.000	0.000	0.000	60.047	18.899	13.289	0.000	0.412	4.462	6.430	3.274	5.632
15	0.000	0.000	0.000	61.353	18.829	4.795	1.416	13.539	8.069	33.184	4.116	0.000
16	0.000	0.000	13.868	29.099	35.033	2.209	0.000	0.000	0.000	4.273	11.974	0.351
17	0.000	0.000	9.862	56.396	11.917	0.644	0.000	0.180	0.425	16.761	0.644	0.000
18	0.000	0.000	9.476	18.330	4.957	14.179	0.622	0.000	0.548	37.650	1.091	0.000
19	0.000	0.000	7.341	35.042	12.877	0.000	2.831	12.947	0.000	0.456	3.349	2.551
20	0.000	0.000	17.462	8.052	12.522	0.000	0.000	0.000	4.313	41.393	0.000	0.000
21	0.000	0.000	0.000	48.752	14.245	3.059	0.000	0.000	2.393	7.271	3.844	0.000
22	0.000	0.000	12.623	25.820	3.305	0.425	0.000	10.050	0.000	31.229	0.000	0.000
23	0.000	0.000	14.245	0.000	10.186	51.443	10.278	39.088	25.816	14.762	1.438	0.000
24	0.000	0.000	1.972	37.475	4.607	14.074	7.341	9.476	0.000	1.197	2.126	5.606
25	0.000	0.000	23.125	5.435	17.883	37.190	0.000	0.000	0.000	12.803	6.035	1.863
26	2.170	0.000	0.000	43.116	22.169	28.827	1.416	26.947	0.189	26.394	9.665	0.000
27	0.000	0.000	0.000	56.133	43.558	18.049	0.000	5.685	27.793	15.078	2.253	1.477
28	0.000	0.000	14.622	33.990	15.568	19.767	0.000	4.918	0.000	0.456	3.349	2.551
29	0.000	0.000	17.462	8.052	12.522	0.000	0.000	0.000	4.313	41.393	0.000	0.000
30	0.000	0.000	0.000	48.752	14.245	3.059	0.000	0.000	2.393	7.271	3.844	0.000
Averages by month:												
	0.072	0.997	10.011	31.452	15.885	11.560	2.170	8.948	5.445	14.423	4.338	0.805

Overall average= 8.842

Table S1-1. Infiltration rates over warming period in inches/year.

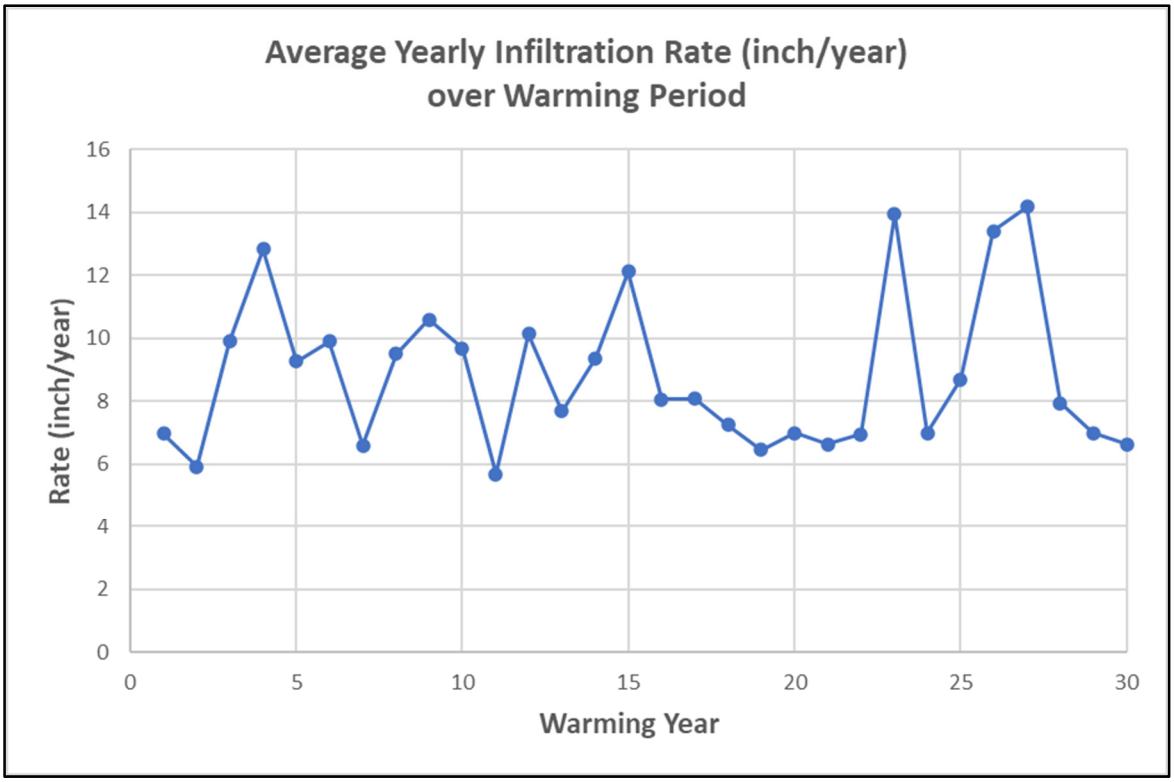

Figure S1-2. Average yearly infiltration rate over warming period.

The temperature series is comprised of a seasonal pattern, a warming trend, and random noise. The seasonal oscillation consists of monthly temperatures that are at a minimum in winter months (0.62°C), increase through the spring, at a maximum in summer (17.62°C), and decrease through the fall (Figure S1-3). The average temperature for each yearly cycle is 8.55°C, corresponding to a cool temperate regime. For the warm-up period, the linear increase is 0.0025°C per month, summing to 0.9°C over 30 years. The warming

is complicated by random noise modeled on a uniform distribution centered on zero and varying between -2 and +2°C (Figure S1-4).

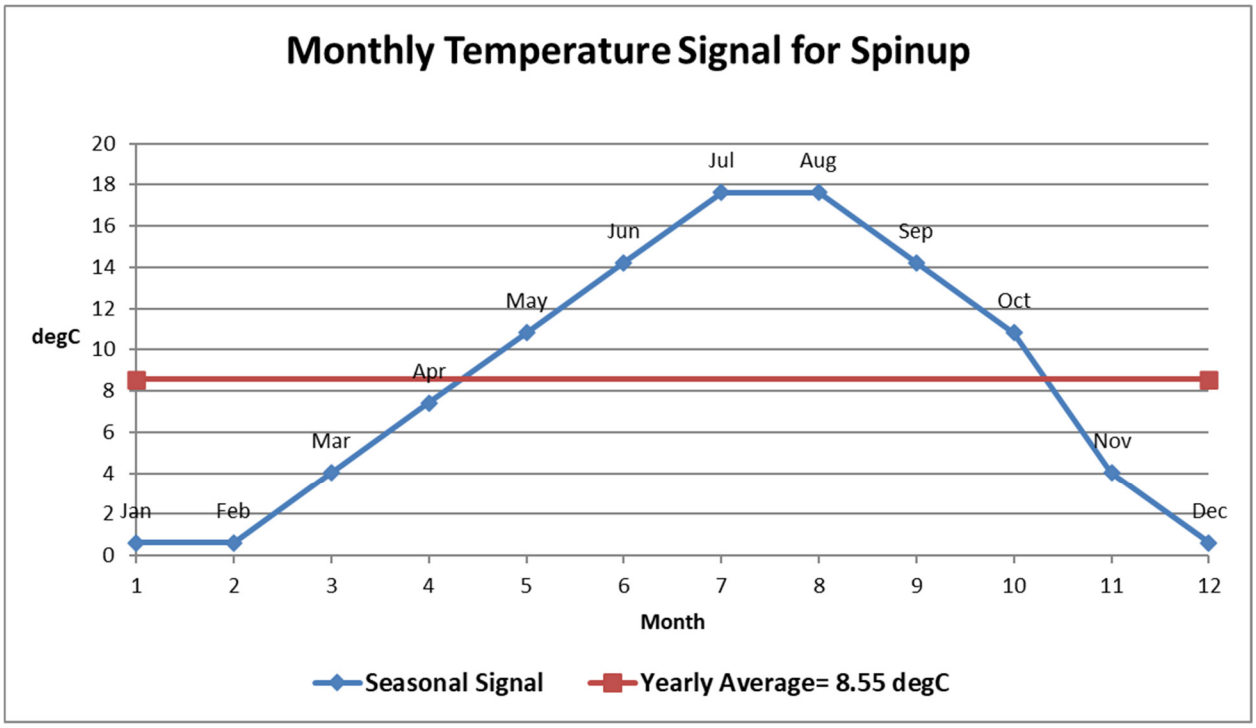

Figure S1-3. Monthly temperature signal for spin-up.

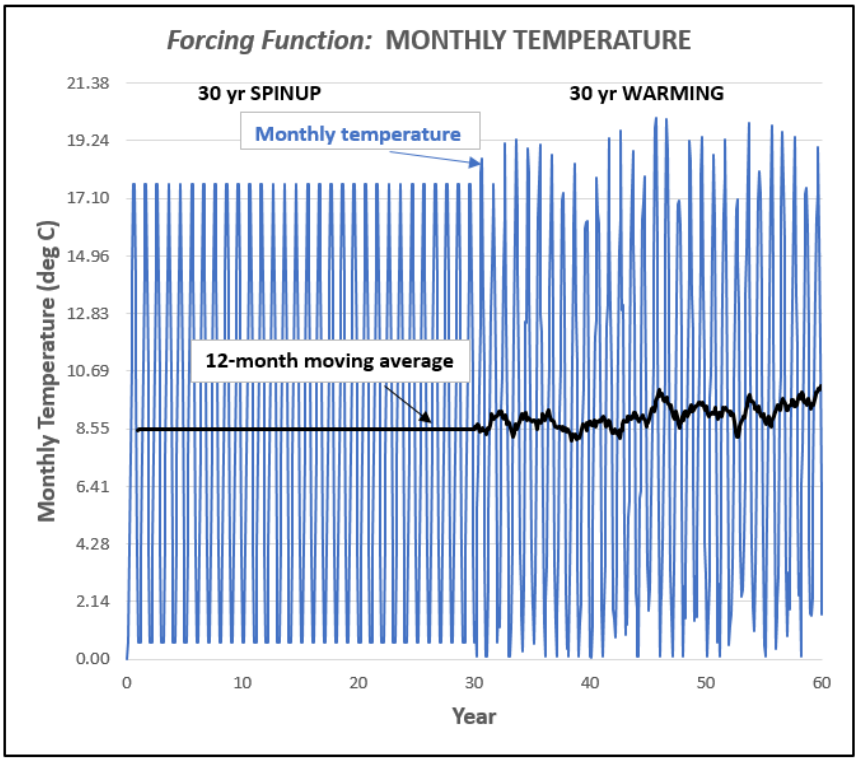

Figure S1-4. Forcing function component: Monthly temperature.

The 12-month moving average displays a modestly increasing temperature trend. The ending 12-month window of the 12-month average corresponds to 10.14°C, about 1.6°C above the spin-up average of 8.55°C. The application of random noise introduces a

slight one-sided bias in the warming period time series because random decreases of monthly temperature below 0°C are reset to 0.1°C. It is also worth noting that both the spin-up and warming time series could be increased by a constant value for each month (for example, increasing all monthly entries of both series by 5°C to bring it more in line with a typical temperate temperature profile in the northern United States). A constant-value increase each month would not change in any way the substantive conclusions drawn from the analysis with respect to the filtering effects of the unsaturated zone in moving heat to the water table and the buffering effects of the groundwater system in conveying heat to streams.

The heat forcing imposed by the model depends on the interaction of infiltration rate and infiltration temperature. In the model, their *product* is effectively translated into units of energy/time, but for the purposes of illustration, the product can be expressed as a dimensionless ratio of the product of the temperature time series for any month to the background product of spin-up and warm-up average temperatures [8 inch/year × 8.55°C, respectively]. The resulting relative heat influx ratio (Figure S1-5) shows the seasonal oscillations around a stationary average present in the spin-up period and the highly variable pattern in the warming period subject to a modest overall increase.

The hypothetical behavior over time emerges more clearly if yearly averages are plotted (Figure S1-6). The ratio of relative heat influx for a given year is as low as 0.5 and as high as 2.5; the overall tendency in this realization is upward with high relative heat influx around the 23rd–27th year of warming, but random components resulting in declining ratios for the final years in the series. On a monthly basis, the relative heat influx behavior is very different in the spin-up than in the warming period (Figure S1-7).

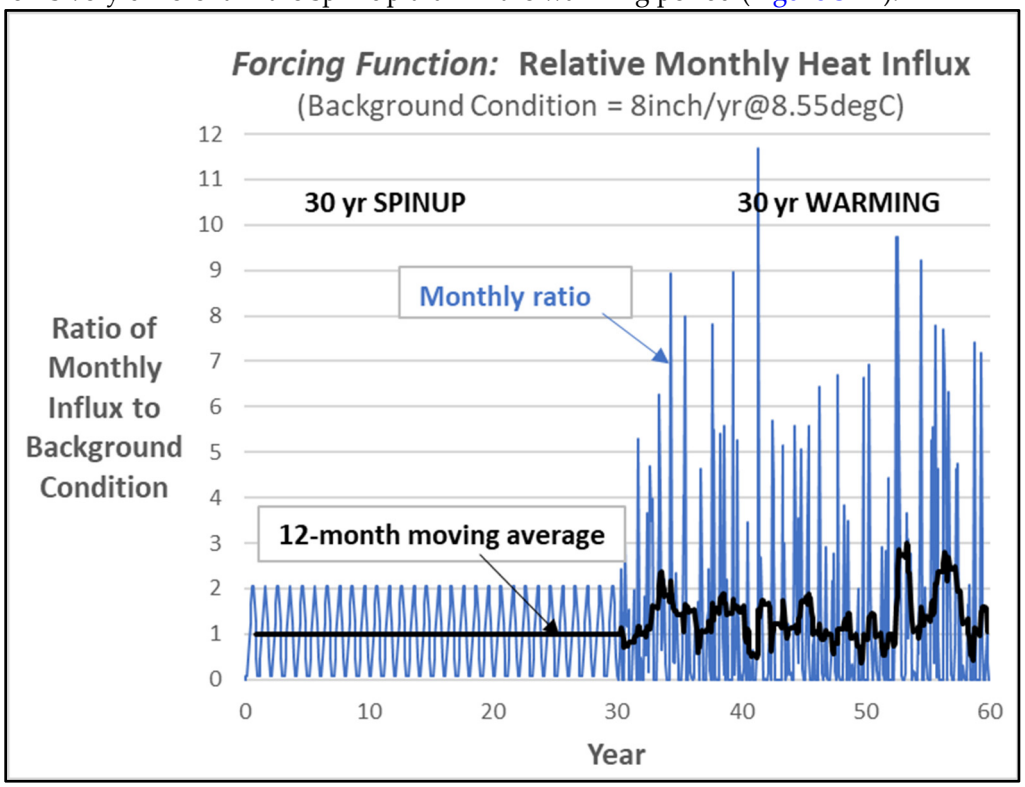

Figure S1-5. Forcing function component: Relative monthly heat influx.

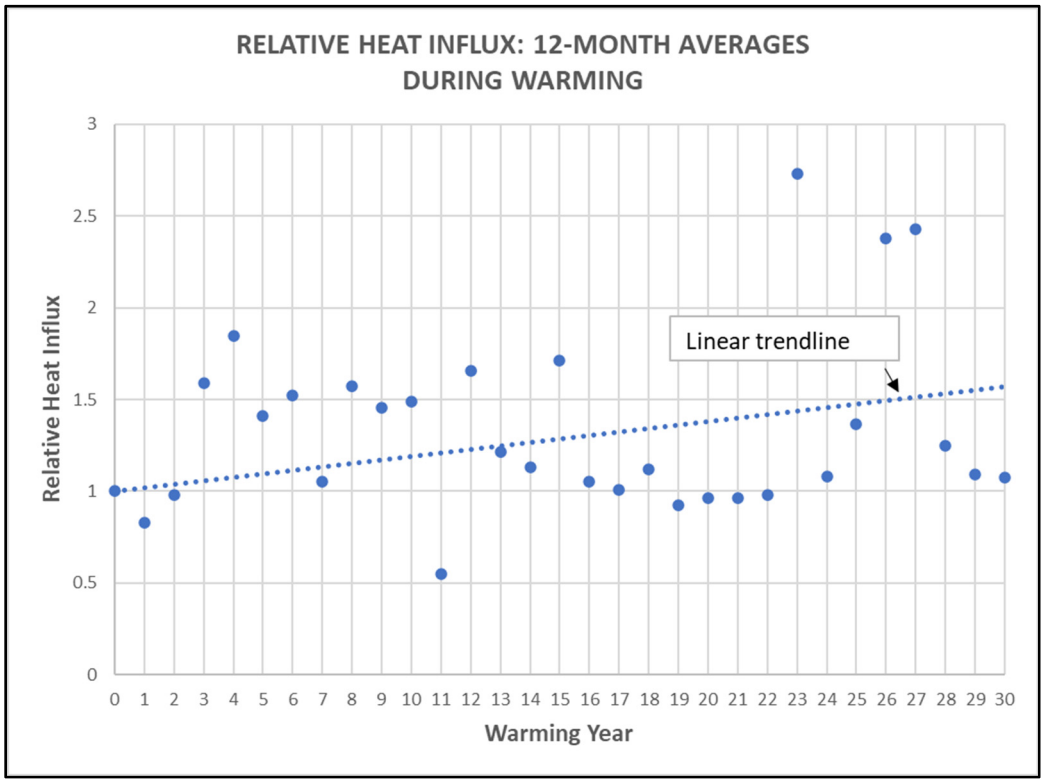

Figure S1-6. Relative heat influx: 12-month averages during warming.

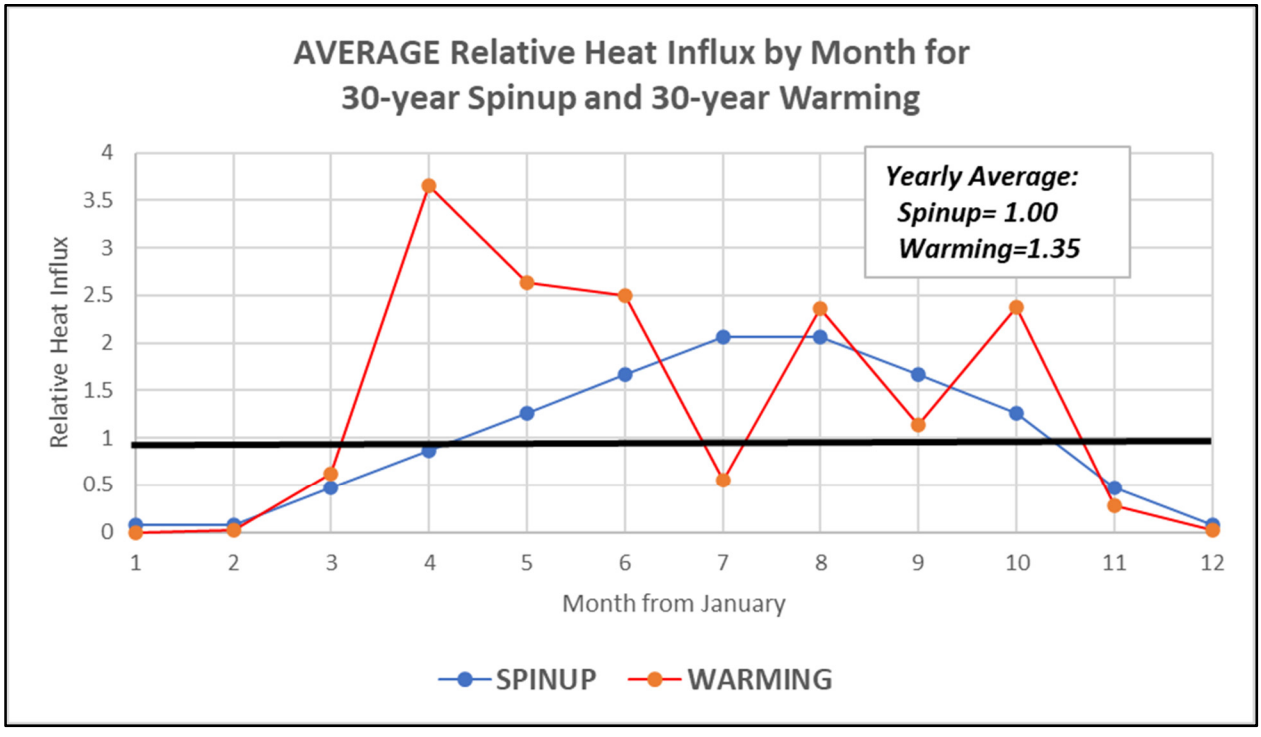

Figure S1-7. Average relative heat influx by month for 30-year spinup and 30-year warming.

Groundwater Model Construction

General head boundary conditions were used on the northern and southern perimeters of the model domain. The resulting regional flow component from the northern to southern boundary is small relative to the transient inflow at the top of the unsaturated zone (UZ), which evolves into recharge. Inflow to the UZ exits the groundwater system

as transient discharge to a series of internal boundary conditions, including a stream network, wetlands and associated drainages, and a lake. The stream network is represented by the MODFLOW SFR package [1], consisting of headwater reaches and tributaries to a main channel that extends from the northern to southern boundary (Figure S1-8). Three large wetlands are located in the western, northern, and eastern parts of the domain, represented by the MODFLOW DRN package [2]. Two additional streams originate at the margin of the western wetland and flow south. A lake is represented by the MODFLOW LAK package [3] (Figure S1-8) and connects with the stream network through a tributary that exits from the downgradient side of the lake. All three surface-water packages–SFR, DRN and LAK–receive groundwater discharge as baseflow, which varies in time and space according to the model solution. The model is configured so that the streams and wetlands only receive baseflow and do not lose surface water to the groundwater system.

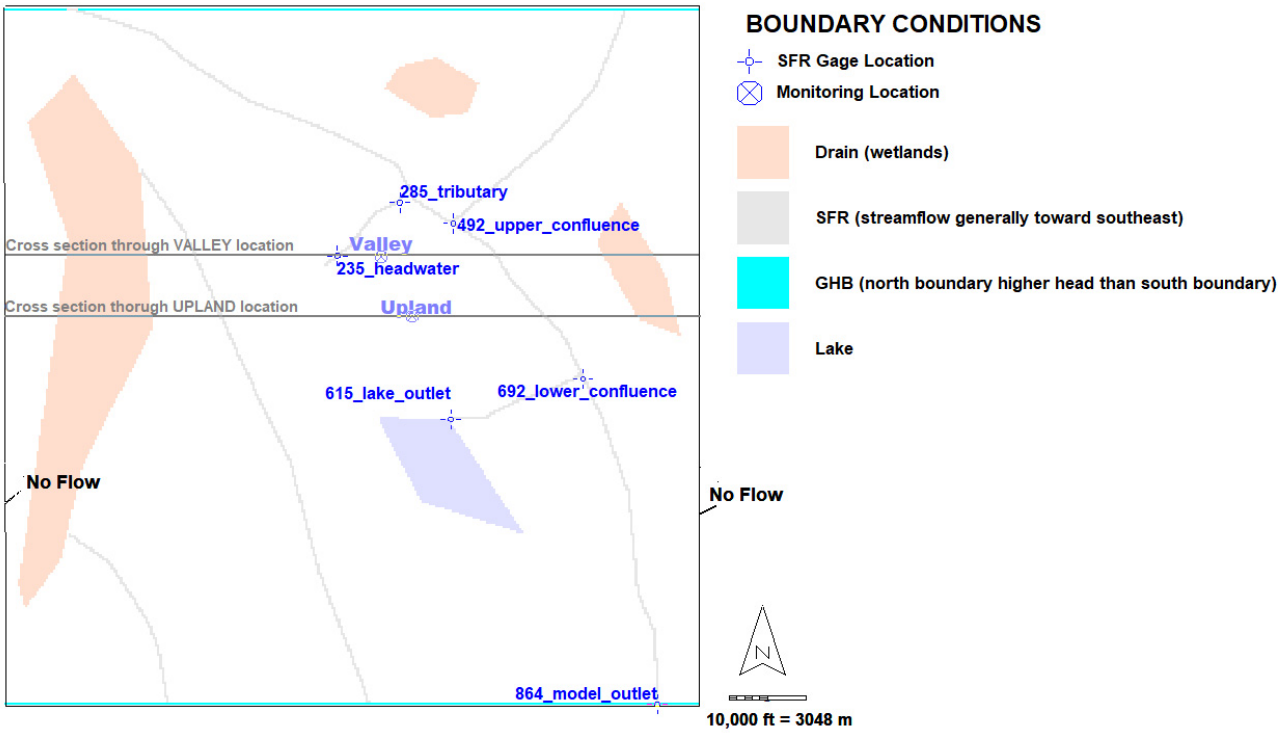

Figure S1-8. Synthetic model. domain, boundary conditions, and locations for simulating temperature.

The presence of the discharge elements produces a complicated flow system with many local groundwater divides whose locations differ with depth, so that a stream segment can draw water from a contributing area influenced by both short flow lines from shallow layers and long flow lines that move up from deeper saturated layers. The water table is also free to oscillate vertically, with oscillations over time on the order of 6 ft (2 m). Despite the strong element of spatial homogeneity in the model, accounting for the effects of the UZ and the configuration of surface-water bodies promotes complexity in the flow system, particularly with a spatially and temporally variable relative heat flux. To evaluate the transient flow and transport results across the watershed, three monitoring well locations and six stream gage locations were selected along the main stream channel (Figure S1-8). The well locations differ with respect to their position in their local basin and their relation to discharge elements, whereas the gages differ with respect to tributary/confluence and upstream/downstream position.

Implementation of Unsaturated Zone Processes

The Unsaturated Zone Flow (UZF) [4] package allows ready calculation of flow from the bottom of the root zone to the water table by replacing the Richards equation with the one dimensional (1D) kinematic wave assumption [5]. The UZF package effectively neglects capillary effects and simulates downward gravitational flow that is controlled by the relation of UZ hydraulic conductivity to transient water content. The kinematic wave formulation is markedly more efficient than solving the full Richards equation and is suited for transient modeling at the watershed scale where capillary and preferential flow effects are secondary to the downward movement of (often overlapping) wetting fronts [6]. Using a Methods of Characteristics solution [7] and discretization of the vertical dimension of the model domain above the water table, UZF partitions infiltrating water into evaporation, unsaturated zone storage, and recharge. The package allows for discharge of groundwater to the land surface, typically as seepage in riparian corridors and around water bodies (see, for example, Feinstein et al. (2020) [8]). The UZF package also accounts for Hortonian-Dunnian rejected infiltration when the infiltration rate exceeds the soils capacity to move water or when the UZ zone becomes saturated. The rejected water and the land-surface seepage can be routed along the topography to the surface-water network as instantaneous groundwater discharge to land surface that subsequently behaves as runoff, often representing, especially in areas of shallow water tables, an important component of the groundwater budget at the watershed scale [8].

In this study, evaporation is neglected because the monthly infiltration rate applied to the top of the UZ is adjusted for root zone ET. Transient changes of UZ storage in response to ongoing infiltration and changing rates of downward movement of wetting fronts toward the water table are responsible for recharge lags. The heat signal carried by infiltrating water and propagated through the groundwater flow system is also affected by the action of the UZ as a low-pass filter of seasonal cycles and longer-term infiltration trends. The flow capabilitiesof the UZF package may be combined with the functionalities offered by MT3D-USGS [9] to directly simulate the propagation of heat through unsaturated and saturated zones, from water entry at the top of the UZ to water discharge from the subsurface. Heat propagation in the UZF and MT3D-USGS coupled model is characterized both in terms of water temperature (the subject of this article) and of energy transmission (the subject of a companion paper, Feinstein et al. (2022) [10]).

A key aspect of the proposed method is that heat propagation in the UZ can be represented in terms of 1D downward movement corresponding to the mathematics of the UZF package. Heat propagation in the saturated zone is simulated as three-dimensional process in MODFLOW, including lateral and upward flow to discharge zones (calculated by means of the MODFLOW sink/source packages). The MODFLOW system of equations is solved using the Newton-Raphson method in the MODFLOW-NWT version of the code [11]. However, transport in the UZ requires a different vertical discretization paradigm than that used to simulate groundwater-surface water flow.

The model layering scheme yields three types of conditions in terms of saturation. For any given row/column location at any given time, the stack of layers can contain cells that are 1) unsaturated, 2) partly saturated, and 3) fully saturated. Water table cells are in the second category and, given the absence of perched conditions in these simulations, there is only one partially unsaturated/partially saturated cell per stack. If the water table falls, for example, in layer 3, then the top receptor layer 1 and layer 2 are unsaturated and layers 4-8 are fully saturated. The layering scheme was designed so that the water table elevation would most often be toward the top of its cell thickness. Different parameters and processes come into play for both the flow and transport solutions depending on the saturation status of the cell.

The flow model solution in MODFLOW-NWT determines the elevation of the water table across the model domain and, accordingly, the distribution of layers where the water table resides. Fig. S1-9 contains cross sections through the UPLAND and VALLEY locations showing the relation of the water table to model layers for the three model versions

representing no simulation of the UZ (NO_UZ_THK), moderately thick UZ (MID_UZ_THK), and thick UZ (HI_UZ_THK). Areas where the water table is in layer 1 at a particular time are called "riparian", as opposed to areas designated as "valley" (water table in layer 2 or 3) and "upland" (water table in layer 4). Because of the moderate land-surface slope upward from surface-water bodies, the water table in the MID_UZ_THK version is found in layer 1 in 20% or more of the model domain, whereas for the HI_UZ_THK version the value is consistently less than 5% (see Table S1-2 for results at selected times and seasons during warming). This difference arising from the contrasting thickness pattern of the UZ between models is important. Heat propagation to the water table in layer 1 without filtering by the UZ is likely to transmit in a flashy manner, particularly during warm and wet months from riparian locations closely connected to streams. However, the infiltration signal in areas of thick UZ will be subjected to lags and dampening. As a secondary effect, the contrasting thicknesses of the three models dictate the amount of seepage that occurs to the land surface–in the MID_UZ_THK version there is relatively more seepage to riparian areas across time, whereas in the HI_UZ_THK version there is relatively more direct discharge to the stream channels and surface-water bodies.

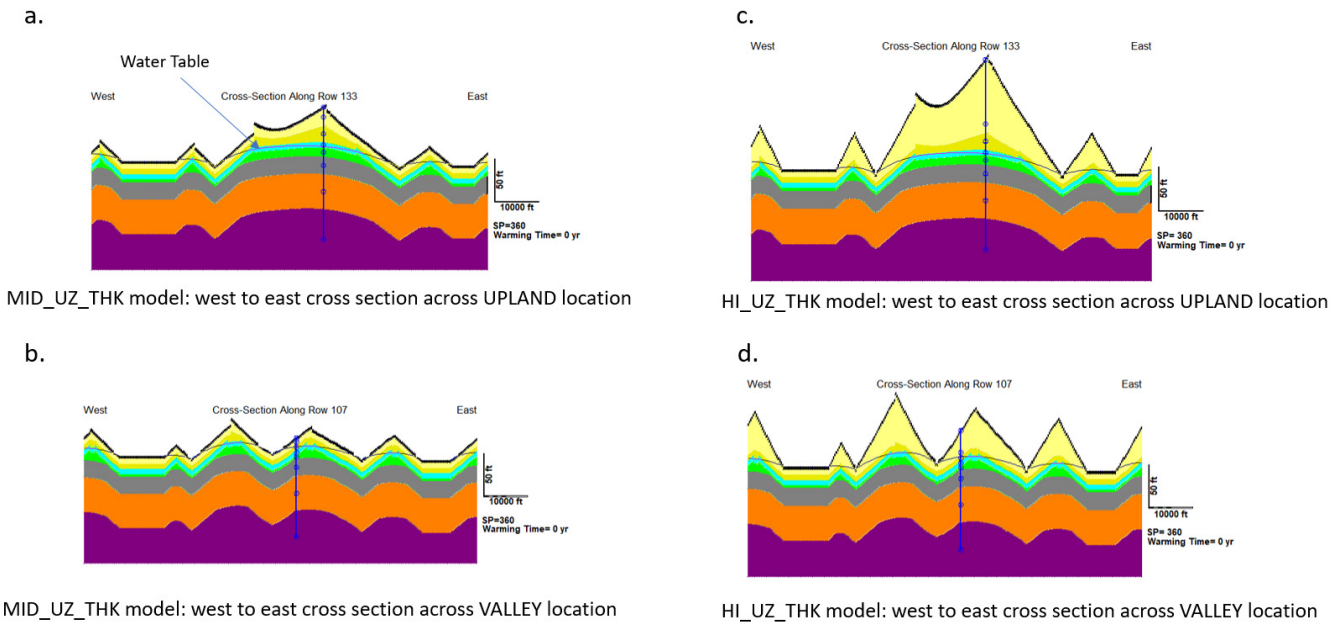

Figure S1-9. Model layering (colors) and water-table elevation for UPLAND and VALLEY locations at end of spin-up period, a. MID_UZ_THK, UPLAND cross section, b) MID_UZ_THK, VALLEY cross section, c) HI_UZ_THK, UPLAND cross section, d) HI_UZ_THK, VALLEY cross section. Vertical layering for MID_UZ_THK model also applies to NO_UZ_THK model.

Vertical distribution of water-table elevations and corresponding temperatures at selected times during warming.

Note: RIPARIAN=> Water Table in Layer 1; VALLEY=> Water Table in Layers 2 or 3; UPLAND=> Water Table in Layer 4.
Water body areas excluded: Area as percent of non-water-body domain.

NO_UZ_THK

	..... Percent Area			.... Average Temperature		
WARMING YR	RIPARIAN-% AREA	VALLEY-% AREA	UPLAND-% AREA	RIPARIAN-AVE	VALLEY-AVE	UPLAND-AVE
0.00 (end SPINUP)	24.0	48.3	27.7	8.44	8.45	8.47
2.75 (Sep)	24.2	45.8	29.9	8.98	8.92	8.98
10.17 (Feb)	28.5	61.9	9.6	8.64	8.56	8.69
15.17 (Feb)	28.2	60.7	11.1	8.89	8.82	8.86
24.67 (Aug)	27.8	55.8	16.4	9.30	9.29	9.31
25.67 (Aug)	33.0	60.4	6.6	9.95	9.92	9.90
30.00 (Dec)	26.2	59.6	14.2	9.31	9.28	9.22

MID_UZ_THK

	..... Percent Area			.... Average Temperature		
WARMING YR	RIPARIAN-% AREA	VALLEY-% AREA	UPLAND-% AREA	RIPARIAN-AVE	VALLEY-AVE	UPLAND-AVE
0.00 (end SPINUP)	20.0	46.7	33.4	8.45	8.59	8.59
2.75 (Sep)	19.9	45.0	35.1	9.02	8.90	8.66
10.17 (Feb)	22.2	64.3	13.6	8.66	8.94	8.97
15.17 (Feb)	22.8	62.4	14.7	8.92	8.97	8.94
24.67 (Aug)	22.2	64.2	13.6	9.28	9.37	9.23
25.67 (Aug)	26.1	48.2	25.7	9.91	9.56	9.23
30.00 (Dec)	20.5	57.6	21.9	9.30	9.43	9.40

HI_UZ_THK

	..... Percent Area			.... Average Temperature		
WARMING YR	RIPARIAN-% AREA	VALLEY-% AREA	UPLAND-% AREA	RIPARIAN-AVE	VALLEY-AVE	UPLAND-AVE
0.00 (end SPINUP)	3.5	51.6	44.9	8.54	8.59	8.55
2.75 (Sep)	3.5	39.1	57.4	8.99	8.81	8.59
10.17 (Feb)	4.8	90.4	4.8	8.68	8.94	8.81
15.17 (Feb)	4.3	85.7	10.0	8.91	8.95	8.85
24.67 (Aug)	4.9	72.3	22.8	9.21	9.27	9.03
25.67 (Aug)	4.8	74.9	20.3	9.84	9.34	9.05
30.00 (Dec)	3.9	87.8	8.3	9.28	9.39	9.25

Table S1-2. Vertical distribution of water-table elevations and corresponding temperatures at.selected times during warming. Units for average temperature are degrees Celsius.

Overall, the distinct land-surface configurations yield different distributions for the depths to the water table for the MID_UZ_THK and HI_UZ_THK flow solutions (see Figure S1-10 for depths at end of the spin-up period mapped across the domain and tabulated at selected locations). The contrasting UZ thicknesses have important implications for the propagation of heat. For example, for the NO_UZ_THK model, the UZ is absent, no dampening occurs, and the top active layers is always a water-table layer. That is, the depth to the water table is zero everywhere across the entire model domain. A9hisgh this assumption is unrealistic, the NO_UZ_THK model is included to evaluate the effect of neglecting the UZ on the heat flux solution and the timing of temperature changes at the water table and at surface-water discharge points.

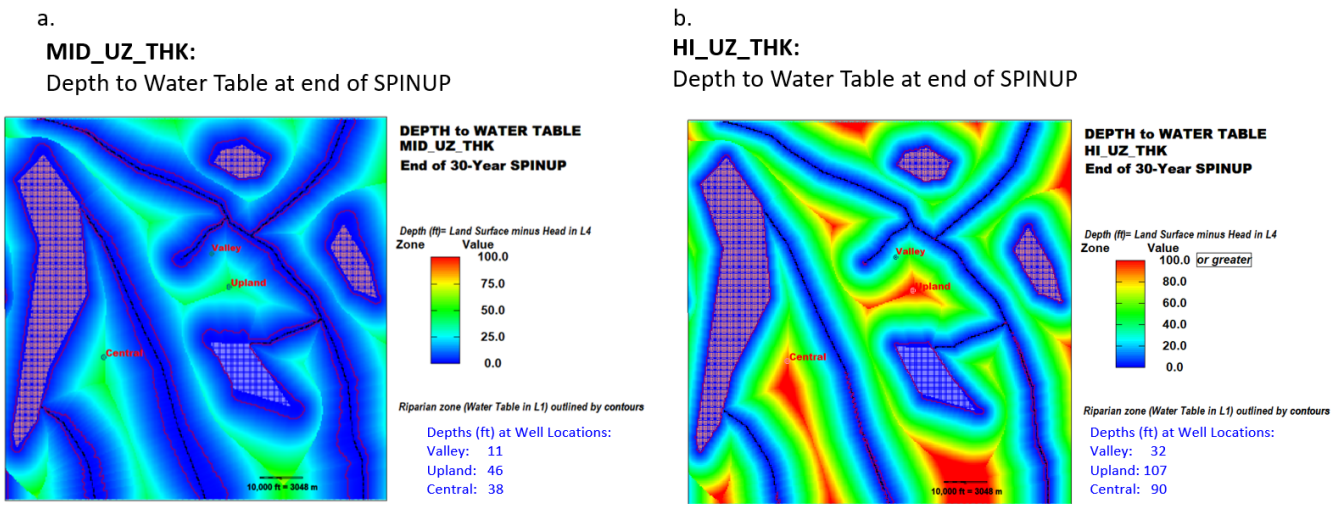

Figure S1-10. Depth to water table at end of spin-up, a) **MID_UZ_THK**; b) **HI_UZ_THK.**

References

1. Niswonger, R.G.; Prudic, D.E. *Documentation of the Streamflow-Routing (SFR2) Package to Include Unsaturated Flow Beneath Streams—A Modification to SFR1*; 2328-7055; U.S. Geological Survey, Techniques and Methods 6-A13; U.S. Geological Survey Scientific: Reston, VA, USA, 2005. https://doi.org/10.3133/tm6A13.
2. Harbaugh, A.W. MODFLOW-2005, the U.S. Geological Survey Modular Ground-Water Model: The Ground-Water Flow Process; U.S. Geological Survey Scientific: Reston, VA, USA, 2005. https://doi.org/10.3133/tm6A16.
3. Merritt, M.L.; Konikow, L.F. Documentation of a Computer Program to Simulate Lake-Aquifer Interaction Using the MODFLOW Ground-Water Flow Model and the MOC3D Solute-Transport Model; U.S. Geological Survey Water-Resources Investigations Report 00–4167; U.S. Geological Survey Scientific: Reston, VA, USA, 2000; p. 146. Available online: https://pubs.er.usgs.gov/publication/wri004167 (accessed on 15 May 2020).
4. Niswonger, R.G.; Prudic, D.E.; Regan, R.S. Documentation of the Unsaturated-Zone Flow (UZF1) Package for Modeling Unsaturated Flow between the Land Surface and the Water Table with MODFLOW-2005; 2328-7055; U.S. Geological Survey Scientific: Reston, VA, USA, 2006; p. 62. https://doi.org/10.3133/tm6A19.
5. Niswonger, R.; Prudic, D.E. Comment on "evaluating interactions between groundwater and vadose zone using the HYDRUS-based flow package for MODFLOW" by Navin Kumar, C. Twarakavi, Jirka Simunek, and Sophia Seo. Vadose Zone J. 2009, 8, 818–819. https://doi.org/10.2136/vzj2008.0155.
6. Harter, T.; Hopmans, J.W. (Eds.) Role of Vadose-Zone Flow Processes in Regional-Scale Hydrology: Review, Opportunities and Challenges; Kluwer Academic Publishers: Wageningen, The Netherlands, 2004; pp. 179–208.
7. Smith, R.E., Approximate sediment water movement by kinematic characteristics: Soil Science Society of America Journal, 1983, v. 47, p. 3-8.
8. Feinstein, D.T.; Hart, D.J.; Gatzke, S.; Hunt, R.J.; Niswonger, R.G.; Fienen, M.N.J.G. A simple method for simulating groundwater interactions with fens to forecast development effects. Groundwater 2020, 58, 524–534. https://doi.org/10.1111/gwat.12931.
9. Bedekar, V.; Morway, E.D.; Langevin, C.D.; Tonkin, M.J. MT3D-USGS Version 1: A U.S. Geological Survey Release of MT3DMS Updated with New and Expanded Transport Capabilities for Use with MODFLOW; 2328-7055; U.S. Geological Survey Scientific: Reston, VA, USA, 2016. https://doi.org/10.3133/tm6A53
10. Feinstein, D.T.; Hunt, R.J.; Morway, E.D. Simulation of heat flow in a synthetic watershed: Lags and damping across multiple pathways under a climate-forcing scenario. Water 2022, 14, 2810. https://doi.org/10.3390/w14182810.
11. Niswonger, R.G.; Panday, S.; Ibaraki, M. MODFLOW-NWT, a Newton Formulation for MODFLOW-2005; U.S. Geological Survey Scientific: Reston, VA, USA, 2011; p. 44. https://doi.org/10.3133/tm6A37.

Supporting Information Section S2–Additional Discussion of Heat Transport Modeling

The mathematical framework and equations for the treatment of heat transport adopted here at the watershed scale are presented in detail for a one-dimensional system in Morway et al. (2022) [1]. In brief, the method equates the time derivatives of heat storage and sorption on the left-hand side of the governing transport equation with the divergence of heat convection, conduction, and dispersion on the right-hand side of the equation [2]. To account for the action of the unsaturated zone (UZ), water content in the governing equation is variable in time and space. The system of transport equations is solved with the finite-difference method.

All parameters associated with terms on both sides of the governing equation are inputs to the MT3D-USGS code revised for heat transport [1]. Similar to the flow simulation, our quasi-hypothetical approach to exploring the viability of the proposed method at the watershed scale combines infiltration inputs that are *variable in time* with subsurface parameter values that are *homogeneous in space*. Table S2-1 lists the constant parameters applied to all three versions of the base model (referred to as NO_UZ_THK, MID_UZ_THK, and HI_UZ_THK models) that control the processes of thermal convection, thermal diffusion and dispersion in the unsaturated and saturated zones. These constant parameters also govern the routing of heat through lake and stream features. The model units for heat parameters are feet, seconds, kilograms and degrees-centigrade. The kilogram mass unit is converted to energy (Joules) and energy rate (Watts) units by means of appropriate fluid density and fluid heat capacity terms.

MT3D-USGS package: Parameter	Value (English length units)	Value (Metric length units)
BTN:		
Porosity	0.3 (--)	0.3 (--)
DSP, for calculation of bulk thermal conductivity and bulk thermal diffusion		
Saturated thermal conductivity	52,669 Joules*day^{-1}*ft^{-1}*degC^{-1}	2.0 Joules Joules*sec^{-1}*m^{-1}*degC^{-1}
Residual thermal conductivity	13,167 Joules*day^{-1}*ft^{-1}*degC^{-1}	0.5 Joules*sec^{-1}*m^{-1}*degC^{-1}
Fluid density	28.3166 kg/ft^3	1000 kg/m^3
Fluid heat capacity	4183 joules/kg/degC	4183 joules/kg/degC
Residual water content	0.04 (--)	0.04 (--)
DSP, for calculation of hydrodynamic dispersion		
longitudinal dispersivity	3.0 ft	0.91 m
transverse horizontal dispersivity	0.30 ft	0.091 m
transverse vertical dispersivity	0.30 ft	0.091 m
UZT:		
Monthly infiltration temperature	see Figure 4	
RCT, for sorption:		
Bulk density of solid	51.849 kg/ft^3	1830 kg/m^3
Distribution coefficient	2.68x10^{-3} ft^3/kg	7.59x10^{-5} m^3/kg
SSM, for GHB cells:		
Source temperature	Set to 8.55 degC during Spinup. Raised 0.03 degC/year during Warming	
from SFT		
Initial temperature in all reaches	8.55 degC	8.55 degC
from LKT		
Initial lake temperature	8.55 degC	8.55 degC
Precipitation temperature	see Figure 4, temperature same as infiltration except for following months:	
	Apr: +0.5 degC, May: +1.0 degC, Jun: +1 .5 degC, Jul: +2.0 degC,	
	Aug: +1.5 degC, Sep: +1.0 degC, Oct: +0.5 degC	

Table S2-1. Spatially homogeneous transport and heat flux parameters.

Of particular interest are the parameters governing thermal sorption and thermal conduction. Thermal sorption in the MT3D-USGS code is assumed to act instantaneously, portioning the energy between the solid and fluid phases according to a retardation factor

based on a ratio that varies with water content. The corresponding equilibrium retardation isotherm is set equal to the expression [1,3]:

Retardation Factor = 1 + (bulk density/water content)·distribution coefficient

A retardation factor of 1.0 implies that all the heat is in the fluid phase and moves at the same rate as the Darcy advective fluid velocity. A retardation factor of 2.0 implies that half the heat is sorbed to the solid phase, and, therefore, the heat moves at half the advective fluid velocity. At saturation, the retardation factor assumes a constant value that, for the selected parameters values in Table S1-3, is equal to about 1.5. This value applies to all model layers below the water table. Above the water table, the retardation factor is a function of water content. For example, at residual water content (0.04), the retardation factor is 4.5, implying that in the UZ most of the infiltrated heat is sorbed and advection downward to the water table is accordingly slowed. A more typical UZ water content value for the MID_UZ_THK and HI_UZ_THK models is close to 0.10, which for the selected parameters yields a retardation factor of 2.6. The selected parameters are adequate for the hypothetical approach presented in the main article, although literature values suggest that for a quartz-sand system, expected retardation values are closer to 2.0 at saturation and to 4.0 at water contents of 0.10 (Morway et al., 2022) [1].

Thermal conduction in the MT3D-USGS code is represented as a bulk process that balances diffusion of heat fronts in the solid phase (not explicitly simulated) and diffusion in the fluid phase [1]. Field studies indicate that the joint diffusion process can be parameterized by a bulk thermal conductivity term that is a function of water content. Following Healey and Ronan (1996) [4], the field relation for thermal conductance is linearized between a minimum value corresponding to residual water content and a maximum value corresponding to saturation. Assuming a quartz-dominated system, reasonable end values are 0.5 Watts·meters·degrees Celsius (Watts·m·°C) at residual water content and 2.0 Watts·m·°C at saturation below the water table (Figure S2-1). The linearization results in a value close to 1.0 Watts·m·°C at typical solved UZ water contents for the base versions of the synthetic model. Thermal conductance is converted to thermal diffusion when divided by the product of water content, fluid density and fluid heat capacity. Thermal diffusion multiplied by the temperature gradient yields the thermal conduction term.

Hydrodynamic dispersion is an additional transport mechanism assumed to behave as a diffusion process and associated with variation of advective velocities at the subgrid scale. A relatively modest longitudinal dispersivity value of 3 ft over the 300-ft grid spacing is assumed for this modeling exercise. Longitudinal dispersivity is multiplied by the thermal gradient to quantify heat propagation by dispersion. Conduction and dispersion occur in all three coordinate directions. Although advection is only downward in the UZ, conduction (and dispersion) can occur in all directions, including upward.

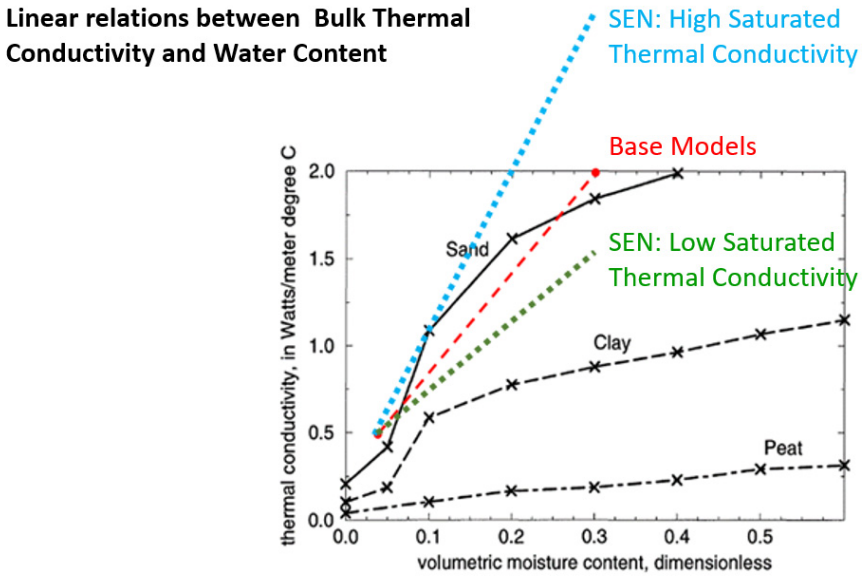

Figure S2-1. Linear relations between thermal conductivity and volumetric moisture content [5]. Thermal conductivity refers to the bulk thermal conductivity and volumetric moisture content refers to the water content.

The heat flux and transport parameters are subject to different degrees of uncertainty in the context of a real field site. To explore the relative importance of this uncertainty on temperature results, sensitivity runs were conducted separately on the following assumed parameter values: UZ vertical hydraulic conductivity, the sorption distribution coefficient, the saturated thermal conductance, and the residual water content. The results are reported below after a presentation of the base model findings.

The heat flux and transport parameters are input to a version of the MT3D-USGS code [1] which simulates both solute and thermal energy transport through the UZ using the UZT package and also through stream and lake surface-water networks using the SFT and LKT packages [2]. Baseflow discharge to surface water–in the form of direct discharge, precipitation inflow, and groundwater runoff (seepage plus rejected infiltration)–is simulated by integrating all upstream discharge at any downstream point.

References

1. Morway, E.D.; Feinstein, D.T.; Hunt, R.J.; Healy, R.W. New capabilities in MT3D-USGS for Simulating Unsaturated-Zone Heat Transport. *Groundwater* **2022**. https://doi.org/10.1111/gwat.13256.
2. Bedekar, V.; Morway, E.D.; Langevin, C.D.; Tonkin, M.J. *MT3D-USGS Version 1: A U.S. Geological Survey Release of MT3DMS Updated with New and Expanded Transport Capabilities for Use with MODFLOW*; 2328-7055; U.S. Geological Survey Scientific: Reston, VA, USA, 2016. https://doi.org/10.3133/tm6A53.
3. Zheng, C.; Wang, P.P. *MT3DMS: A Modular Three-Dimensional Multispecies Transport Model for Simulation of Advection, Dispersion, and Chemical Reactions of Contaminants in Groundwater Systems; Documentation and User's Guide*; Contract Report SERDP-99-1; U.S. Army Engineer Research and Development Center: Vicksburg, MS, USA, 1999. http://hydro.geo.ua.edu/mt3d.
4. Healy, R.W., and A.D. Ronan. *Documentation of computer program VS2DH for simulation of energy transport in variably saturated porous media—Modification of the U.S. Geological Survey's computer program VS2DT.* U.S. Geological Survey Water-Resources Investigations Report 96-4230 36. 1996. https://doi.org/10.3133/wri964230
5. van Duin, R.H.A. *The influence of soil management on the temperature wave near the soil surface.* Wageningen University & Research, Technical Bulletin no. 29, Institute for Land and Water Management Research. 1963. https://edepot.wur.nl/417072

Supporting Information Section S3–Additional Explanation of Simulation and Sensitivity Results and Model Limitations

Difference among the Three Conceptualizations: Heads

The effect of the groundwater flow system on buffering (that is, lagging, dampening and mixing) groundwater temperatures moving from the water table toward surface-water is distinct from the thermal buffering of the unsaturated zone (UZ). The UZ functions as a low-pass filter to flatten high-frequency events and change the phase and amplitude of the recharge temperature with respect to the infiltrating temperature signal at the land surface. The buffering action of the groundwater system in combination with the UZ, together constituting the subsurface system, can be partly captured by examining results in vertical section. The first element affecting heat transfer is the vertical head gradient above and below the water table. Hydrographs of water levels at the UPLAND and VALLEY locations (Figure S3-1) show that the excursion (maximum minus minimum)of heads over the warming period due to variations in infiltration rates is close to 7 ft (2 m) at the UPLAND location and on the order of 4-5 ft (1.5 m) at the VALLEY location (as expected given the dampening effect of the UZ, the transient behavior is flashiest for the NO_UZ_THK version and smoothest for the HI_UZ_THK) but that the vertical head difference is small across layers from receptor layer 1 to layer 8 at the bottom of the saturated system.

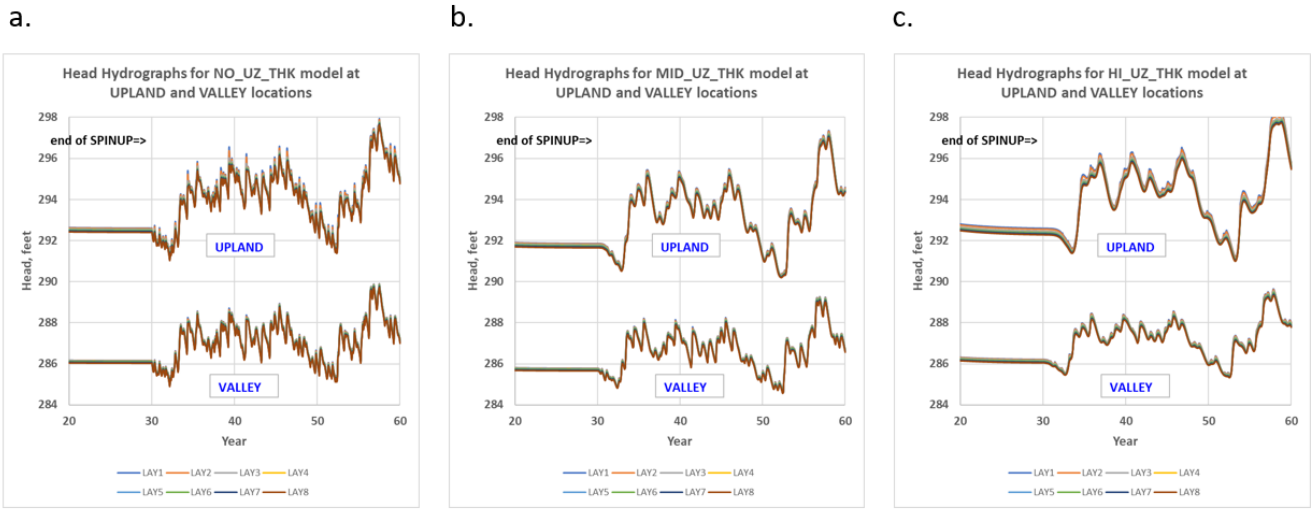

Figure S3-1. Head hydrographs for base model layers 1-8 at UPLAND and VALLEY locations, a. **NO_UZ_THK**; b. **MID_UZ_THK**; c. **HI_UZ_THK**.

Consider head conditions at the end of the spin-up period. Taking the vertical head gradient between the center elevation of model layer 4 (L4) and the center elevation of L8 as indicative of the saturated part of the flow system, all three base models show a vertical gradient of 1.2×10^{-3} at the UPLAND location and a vertical gradient of 1.1×10^{-3} at the VALLEY location. Taking the vertical head gradient between the center elevation of L1 and the center elevation of L4 as indicative of conditions in the UZ, both the MID_UZ_THK and HI_UZ_THK versions show vertical gradients of 1.8×10^{-3} at the UPLAND location and 1.7×10^{-3} at the VALLEY location (note that the shallow layers are typically inactive for the NO_UZ_THK model.) The close agreement of vertical gradients and uniformity of vertical hydraulic conductivity values across the base model versions suggest that for the hypothetical scenarios the differences in temperature results at the water table and in streams is more closely tied to transport lags associated with UZ thickness and subsequent dampening along deeper groundwater paths than it is to the distribution of simulated vertical velocities in the system.

Difference among the Three Conceptualizations: Heat in Cross Section

An additional characterization of vertical profiles in the synthetic base models can be viewed in terms of temperature cross sections (Figure S3-2) oriented along the model (west to east) row that intersects the UPLAND location (trace shown in Figure S1-8). On the left of the cross-section plots (Figure S3-2, a-c) are the results corresponding to the month of February 15.17 years after warming has begun–the average relative heat influx ratio for the previous year is equal to 1.71 with zero heat influx for February. The plots show a modest vertical temperature gradient from the land surface to the water table and from the water table to the model bottom. On the right of the plot (Figure S3-2, d-f) are results corresponding to the month of August 25.67 years after warming has begun–the average relative heat influx for the previous year is high, equal to 2.12, while a very high heat influx ratio of 7.79 for August. The plots indicate about a degree of difference in temperature between the shallow and deep layers. For the time period of 15.17 years, temperatures at and below the water table are similar for the MID_UZ_THK and HI_UZ_THK models at this location, whereas the temperatures for the NO_UZ_THK model are cooler, reflecting the absence of an UZ lag for this model and colder month of February. For the time period of 25.67 years, temperatures at and below the water table are similar for the NO_UZ_THK and MID_UZ_THK models, whereas temperatures for the HI_UZ_THK model are modestly cooler, reflecting the longer time lags typical of the HI_UZ_THK model, slowing the transfer of heat from the land surface.

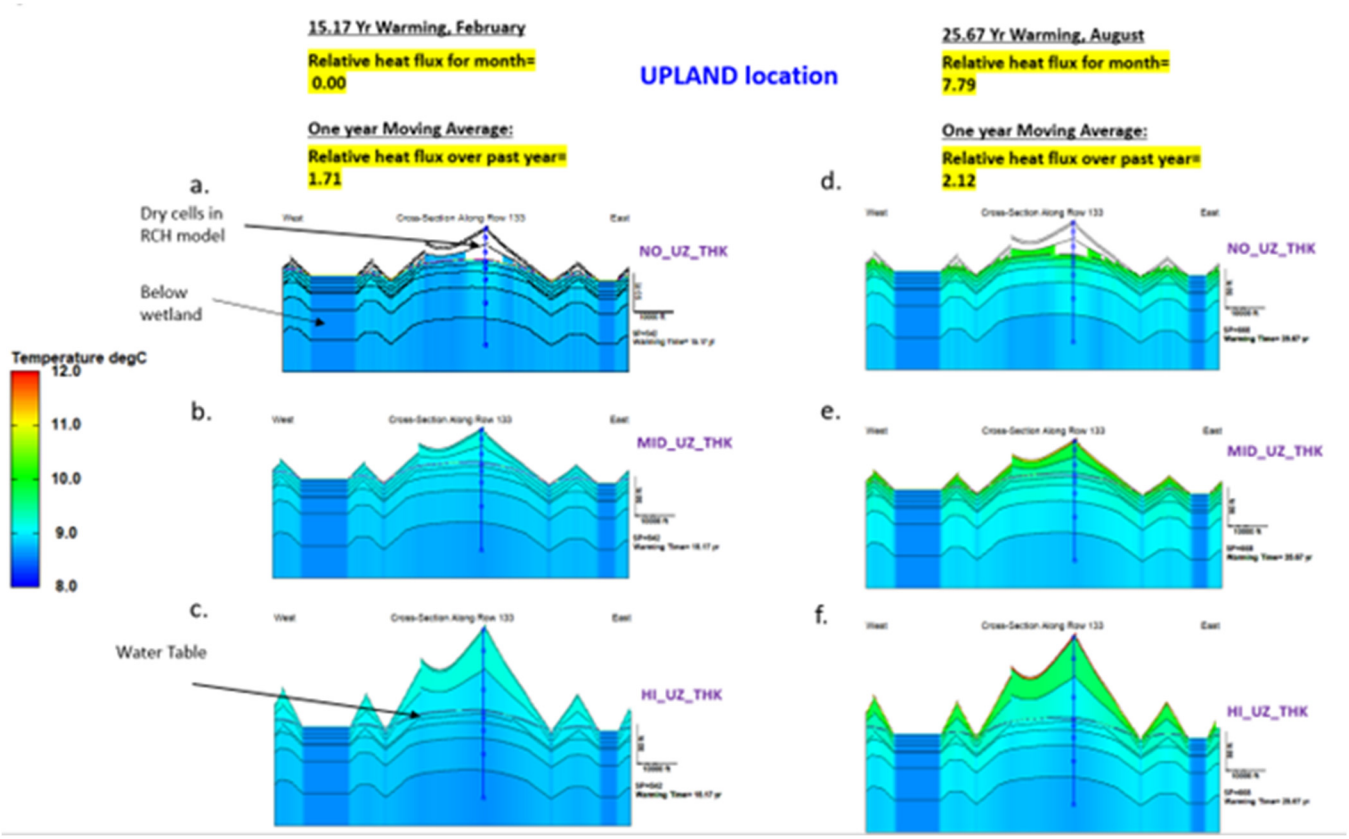

Figure S3-2. Temperature and water-table elevation in cross section through UPLAND location for three base models, layers 1-8, at selected times during warming period, a. NO_UZ_THK, 15.17 years of warming; b. MID_UZ_THK, 15.17 years of warming; c. HI_UZ_THK, 15.17 years of warming; d. NO_UZ_THK, 25.67 years of warming; e. MID_UZ_THK, 25.67 years of warming; f. HI_UZ_THK, 25.67 years of warming. The labels above plots indicate relative heat flux conditions for 15.17 and 25.67 years of warming.

Difference among the Three Conceptualizations: Stream Temperature

Stream temperature results were evaluated using the maximum stream baseflow temperature by year, the temperature results for the month of August, and the temperatures associated with the minimum monthly baseflow by year (Figure S3-3). Among the three test models, the MID_UZ_THK model yields the maximum yearly and August temperatures–particularly at the outlet gage (Figs. S3-3d,e)–despite the filtering effect of the UZ. This result likely follows from the important role of the riparian zone simulated by the UZF1 package in both the MID_UZ_THK and HI_UZ_THK simulation, but with a greater spatial extent in the MID_UZ_THK model. In contrast, during periods of low baseflow to streams at gage locations, all three models yield muted stream temperature responses with little trace of the seasonal forcing and only exhibiting a gradual upward temperature trend (Figs. S3-3c and S3-3f). This result is likely due to the simulated temperature of baseflow to the streams. That is, during low baseflow, the discharge to streams is subjected to greater influence of flow originating from deeper in the groundwater system with long pathlines and residence time in zones that are shielded from warming at the surface.

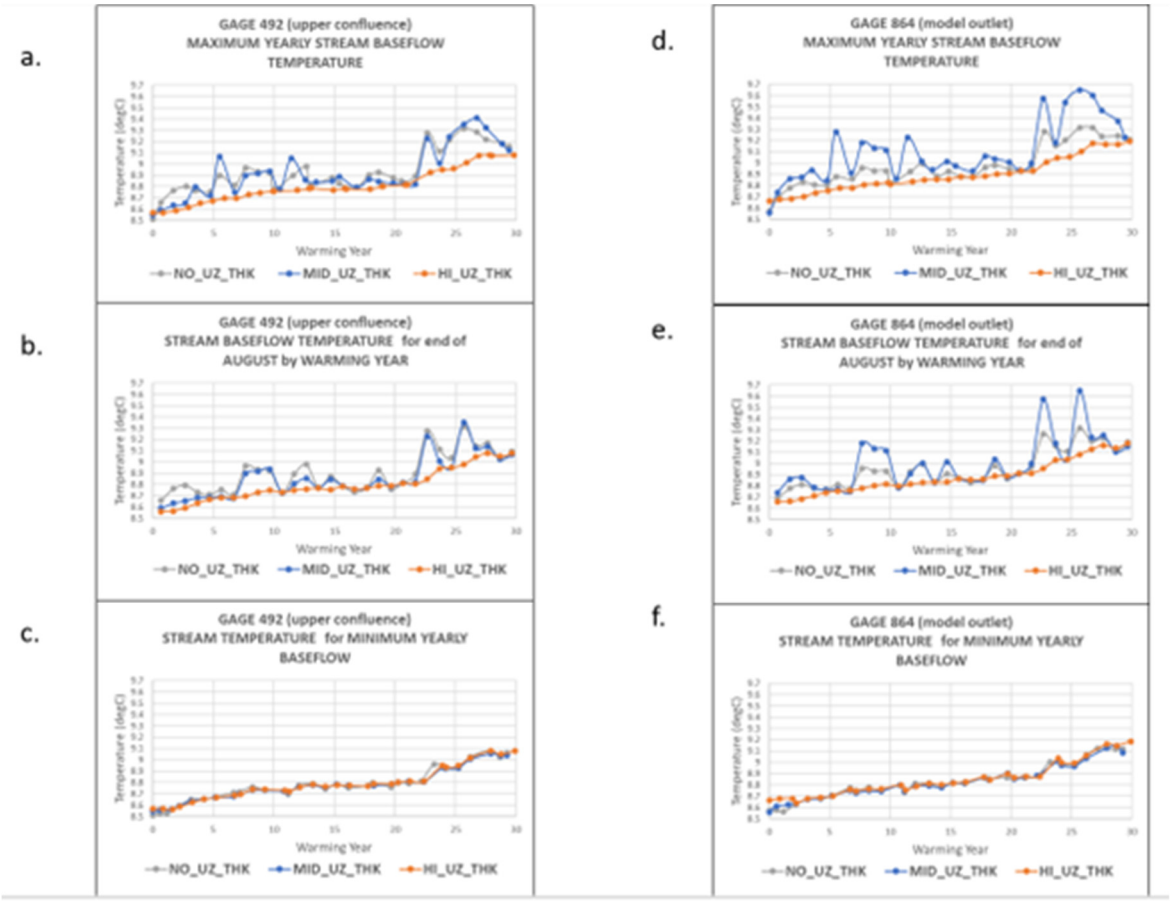

Figure S3-3. Stream baseflow temperature for three base models in response to warming at selected gages, a, d. maximum yearly temperature, b, e. August temperature by year, and c, f. temperature corresponding to minimum monthly baseflow by year. Upper confluence gage shown in a-c; model outlet gage shown in d-f.

Sensitivity of Temperature Results to Model Layering

The layering scheme applied to the base models allows, at any location and at any time, to stack model cells; for example, from top to bottom, unsaturated cells above the water table, partly saturated cells hosting the water table, and fully saturated cells below the water table. The vertical discretization influences the rate of movement of infiltration

downward in the UZ according to the kinematic wave equations for unsaturated flow implemented by the MODFLOW UZF package [1]. The sensitivity of the head and temperature results to the UZ layering scheme adopted can be tested by adding layers near the land surface. To that end, layers 2 and 3 in both the MID_UZ_THK (Figure S3-4,a-d) and HI_UZ_THK (Figure S3-5,a-d) base models were divided in half, increasing the model layer numbers from 8 to 10. The refinement yields thinner unsaturated cells whenever the water table is below layer 2 or layer 3, allowing for more precise representation of the percolation of wetting fronts and associated heat fronts to the water table for both the MID_UZ_THK and HI_UZ_THK thickness models.

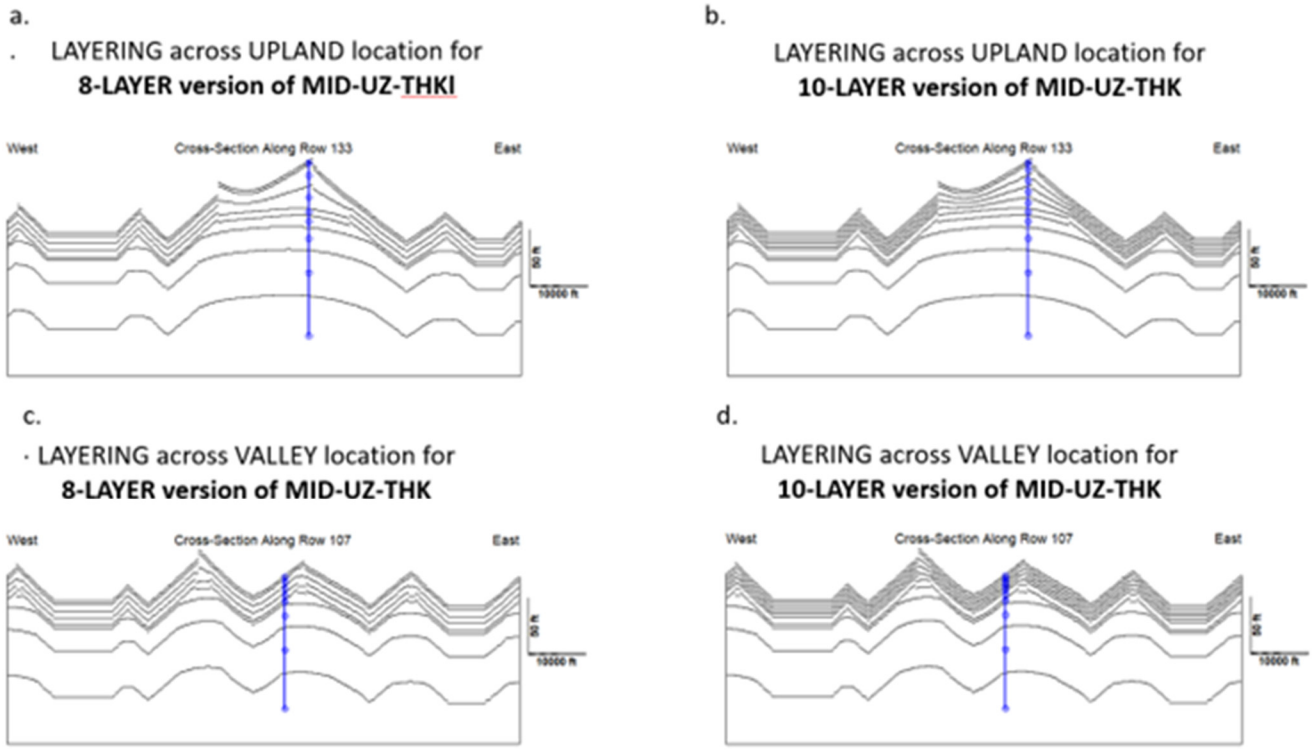

Figure S3-4. Cross sections showing layering for 8-layer base model version and 10-layer revised base model version of MID-UZ-THK, a. 8-layer version for section across UPLAND location; b. 10-layer version for section across UPLAND location c. 8-layer version for section across VALLEY location; d. 10-layer version for section across VALLEY location.

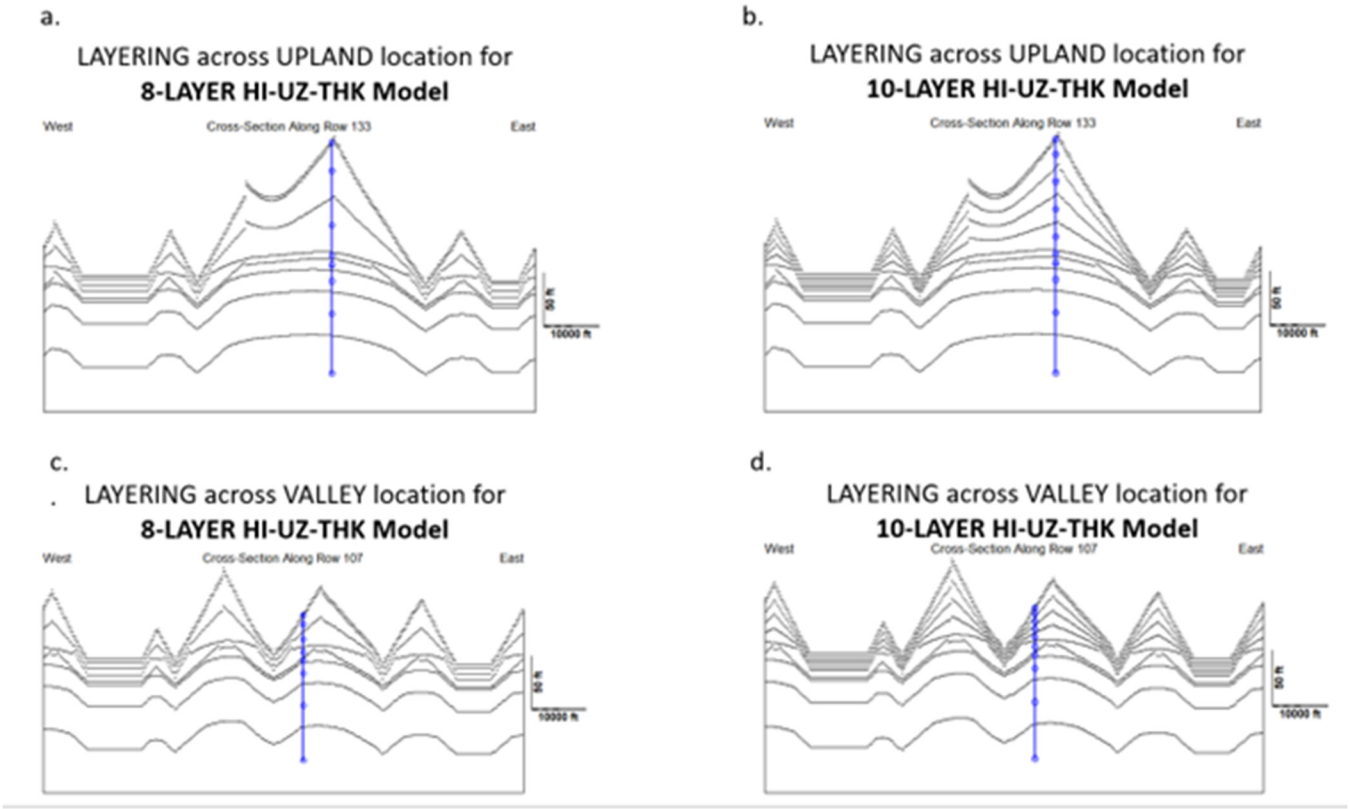

Figure S3-5. Cross sections showing layering for 8-layer base model version and 10-layer revised base model version of HI-UZ-THK**,** a. 8-layer version for section across UPLAND location; b. 10-layer version for section across UPLAND location; c. eight-layer version for section across VALLEY location; d. 10-layer version for section across VALLEY location.

The extra vertical refinement has very little effect on model results in the saturated part of the system. Comparison of the temperature hydrographs at the UPLAND and VALLEY locations for the 8-layer and 10-layer model versions (8L and 10L in Figure S3-6 and S3-7, respectively) indicate negligible difference in the temperature trends for the saturated layers (commonly at or below layer 4 in the 8-layer model and at or below layer 6 in the 10-layer model). Similarly, the refined layering has only a slight effect on the output of the maximum yearly temperatures registered at the model-outlet gage location for either the MID_UZ_THK (Figure S3-8a) or HI_UZ_THK (Figure S3-8b) models. Adding layers tends to diminish the stream temperatures in both models, though only slightly.

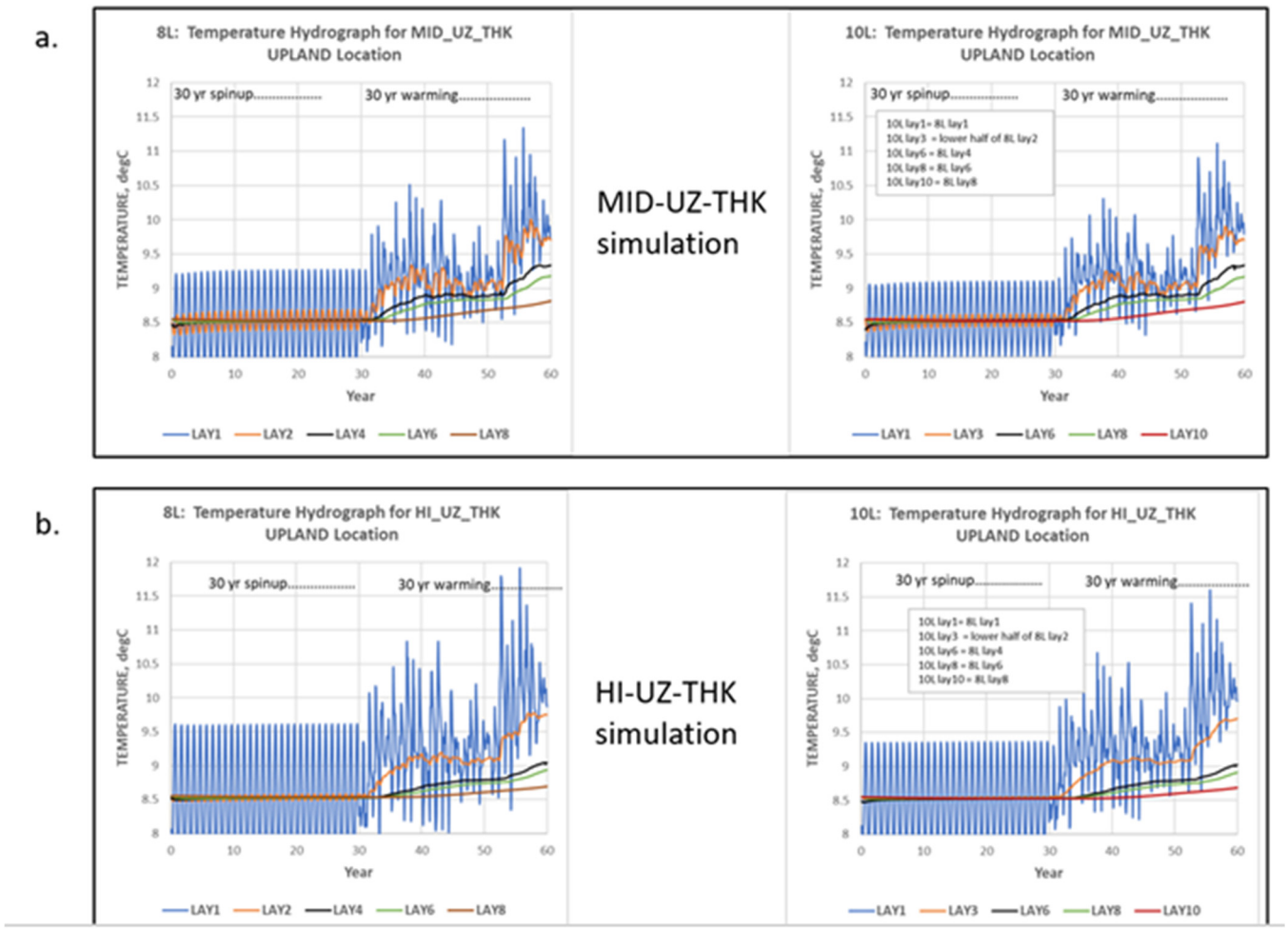

Figure S3-6. Temperature hydrographs comparing results for 8-layer and 10-layer model versions for the UPLAND location, a. 8-layer and 10-layer results for the MID_UZ_THK model, and b. 8-layer and 10-layer results for the HI_UZ_THK model.

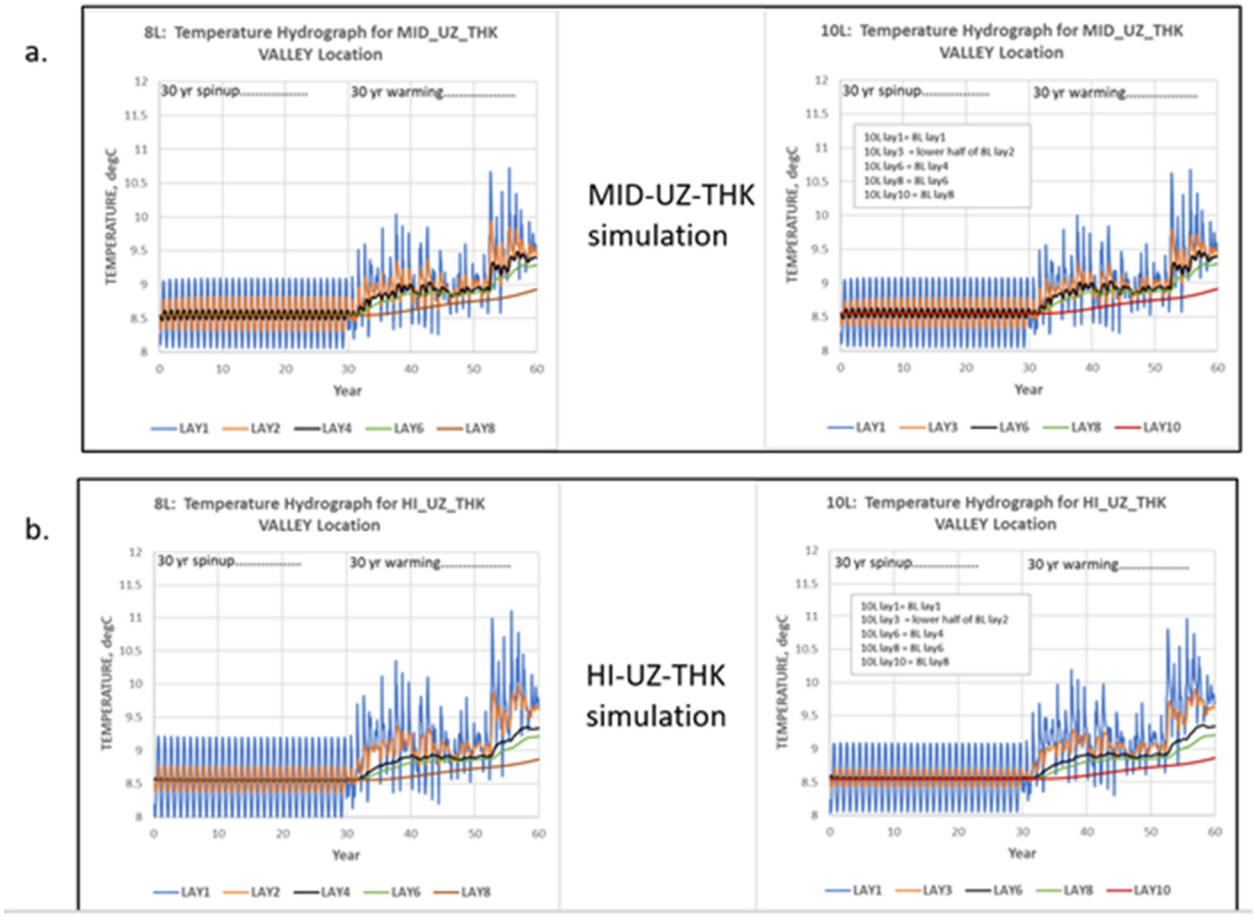

Figure S3-7. Temperature hydrographs comparing results for 8-layer and 10-layer model versions for VALLEY location, a. 8-layer and 10-layer results for the MID_UZ_THK model, and b. 8-layer and 10-layer results for the HI_UZ_THK model.

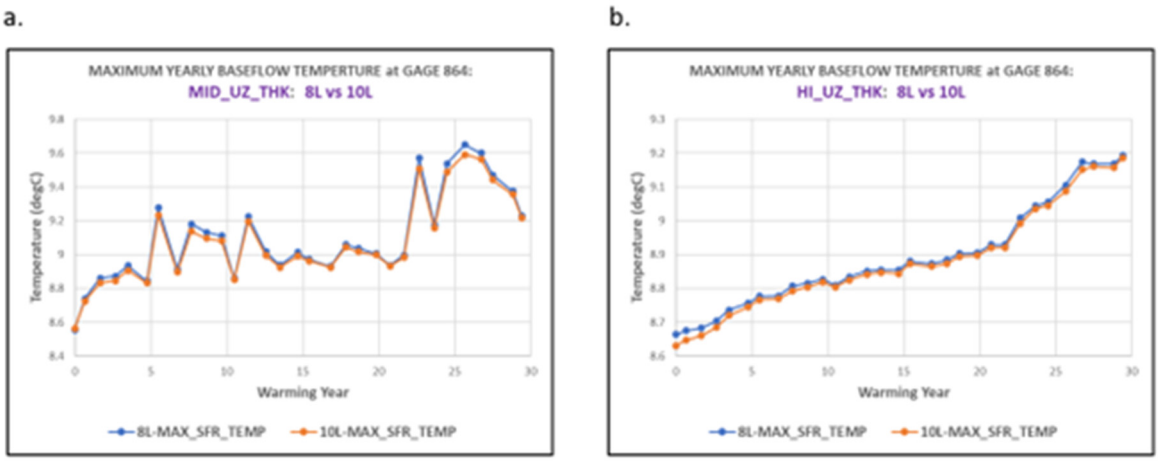

Figure S3-8. Temperature plots comparing maximum yearly temperature for 8-layer and 10-layer model versions at model outlet gage, a. 8-layer versus 10-layer results for the MID_UZ_THK model, and b. 8-layer versus 10-layer results for the HI_UZ_THK MODEL.

Sensitivity of Temperature Results to Model Parameters

Selected model parameter values (Table S3-1) were varied to test the sensitivity of changing values on the distribution of water-table and stream baseflow temperatures. Varied parameters include flow parameters (vertical conductivity in the UZ controlling *percolation*, saturated water content and specific yield controlling the unsaturated and

saturated *storage response*) and heat transport parameters (distribution coefficient controlling *sorption*, saturated thermal conductivity controlling *conduction*). The sensitivity analysis is restricted to the MID_UZ_THK model version.

Run Name	Parameter change	Sensitivity Value
SEN_UZ_KV	UZ Kv reduced by 0.1x	0.1 ft/d (0.305 m/day)
SEN_UZ_KV1	UZ Kv reduced by 0.01x	0.01 ft/day (0.0305 m/day)
SENSorbLo	Distribution coefficient reduced by 0.5x	$1.34x10^{-3}$ ft3/kg ($3.80x10^{-5}$ m3/kg)
SENSorbHi	Distribution coefficient increased by 2.0x	$5.36x10^{-3}$ ft3/kg ($1.52x10^{-4}$ m3/kg)
SENConductLo	Saturated thermal conductivity reduced by 0.5x	26,335 Joules*day^{-1}*ft^{-1}*degC^{-1} (1.0 Joules*sec^{-1}*m^{-1}*degC^{-1})
SENConductHi	Saturated thermal conductivity increased by 1.5x	79,004 Joules*day^{-1}*ft^{-1}*degC^{-1} (3.0 Joules*sec^{-1}*m^{-1}*degC^{-1})
SEN_UZ_thetaS	Saturated water content decreased in both UZ and SAT zone	0.19 (--)
	Specific yield decreased in SAT zone	0.15 (--)

Table S3-1. Summary of changes to parameter values for sensitivity simulations using the MID_UZ_THK base model. The column "Sensitivity Value" indicates the new value tested in each respective sensitivity run.

The percent of the simulated water table above 9.5°C during the 30 years of warming is one indicator of how efficiently heat pulses spread to and across the groundwater system. This threshold represents the proportion of the domain at the water table (omitting areas occupied by wetlands or the lake) registering a degree or more above the background condition. Plots in Figure S3-9 compare–for the month of August–the threshold water-table results for the MID_UZ_THK base model with the corresponding results for the set of varied parameters. The plots indicate a fair amount of parameter sensitivity; for example, reducing the UZ vertical hydraulic conductivity (Kv) by 0.1 has only moderate effect on the domain area above 9.5°C through time, but reducing Kvby 0.01 has appreciable effect, tending to strongly retard the movement of heat through the system (Figure S3-9a). Additionally, lowering sorption leads to more efficient heat propagation, and vice versa (Figure S3-9b). Lowering the value of the saturated thermal conductivity reduces bulk thermal conduction, which, notably, results in more efficient heat propagation through the fluid phase, whereas raising the saturated thermal conductivity has the opposite effect (Figure S3-9c). Lastly, lowering the value of storage parameters accelerates the percolation of heat to the water table and across the groundwater system (Figure S3-9d).

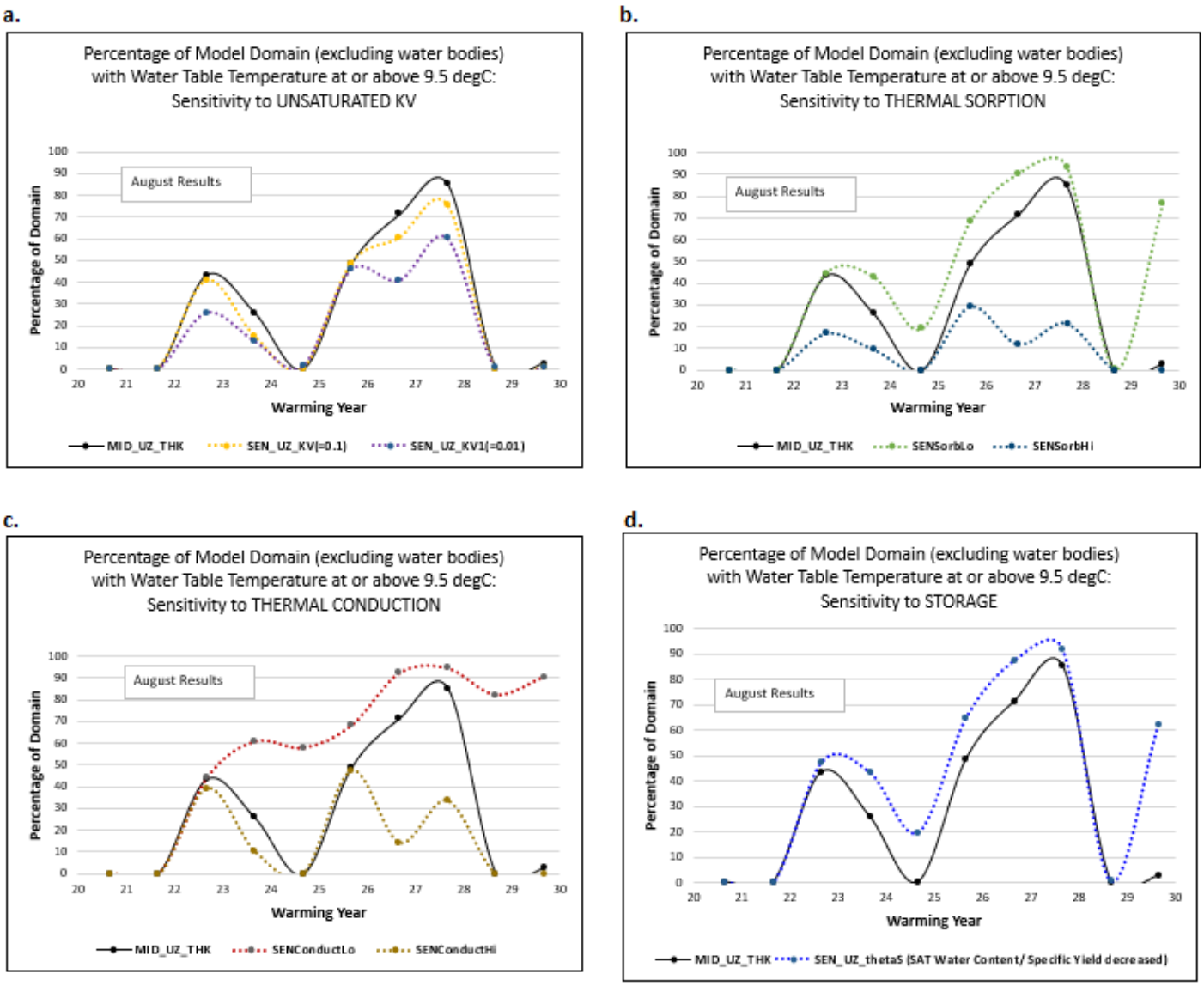

Figure S3-9. Sensitivity results for MID_UZ_THK model as a percentage of model domain for August, by year, with water-table temperature at or above 9.5 °C, a. sensitivity of August results to value of UZ vertical hydraulic conductivity, b. sensitivity of August results to value of distribution coefficient for sorption, c. sensitivity of August results to value of thermal conductivity for conduction, and d. sensitivity of August results to values of UZ and saturated storage parameters. Water body cells excluded from calculation. See Table S3-1 for change to parameter values.

Just as stream baseflow temperatures under simulated warming conditions are buffered with respect to temperature changes near the land surface or at the water table, baseflow temperatures in Figure S3-10 show muted sensitivity to parameter changes. The time series of the stream temperatures at the model-outlet gage (Figure S3-10,a-d) and the results isolated for the month of August during warming (Figure S3-10,e-h) show little separation in terms of frequency or amplitude for the case where UZ Kv is reduced by 0.1x and for reductions or increases to the saturated thermal conductivity term. Lowering the sorption and storage capacity tends to heighten the stream temperature amplitude response. The effect of reducing UZ Kv to 0.01 is more complicated. The time series (Figure S3-10a) show that during some warming months, the stream temperatures in the simulation with lower Kv are higher compared to the original UZ_MID_THK model, but more often they are lower. This anomaly is due to a particular feature of the

MODFLOW/MT3D-USGS codes–the possibility of rejected infiltration (in terms of both water and heat) when the water table is at the land surface (provoking Dunnian overland flow) or when the (monthly) infiltration rate exceeds the imposed UZ Kv (provoking Hortonian overland flow). The codes route the water and heat instantaneously to topographically adjacent streams and lakes as groundwater runoff. The high water-table condition occurs in riparian areas; for the MID_UZ_THK model, this saturated condition leads to rejection of about 1%-4% of the applied infiltration over the warming period. Reducing Kv by 0.1 makes no difference to this rate of rejection and associated groundwater runoff. However, for the synthetic model under study, reducing Kv by 0.0.1 causes about 10%-40% of the applied infiltration to be rejected during certain months over the 30-year warmup. Rejected infiltration is due strictly to the excessive infiltration rate with respect to the low UZ Kv, which occurs for the synthetic model in eleven months that are particularly wet and occur during warm periods. During these months, heat transported from areas undergoing rejected infiltration directly to downgradient stream segments can cause dramatic short-term increases in the heat that arrives at the model outlet (Figure S3-10a). However, when this Hortonian effect is absent, the low UZ Kv term acts mostly in the opposite way, retarding the percolation of heat to the water table and deeper into the groundwater system. These contrary effects are automatically realized in the MODFLOW/MT3D-USGS codes, but it is plausible that they also occur in nature, in real temperate-zone watersheds, at time intervals equal to or less than a month.

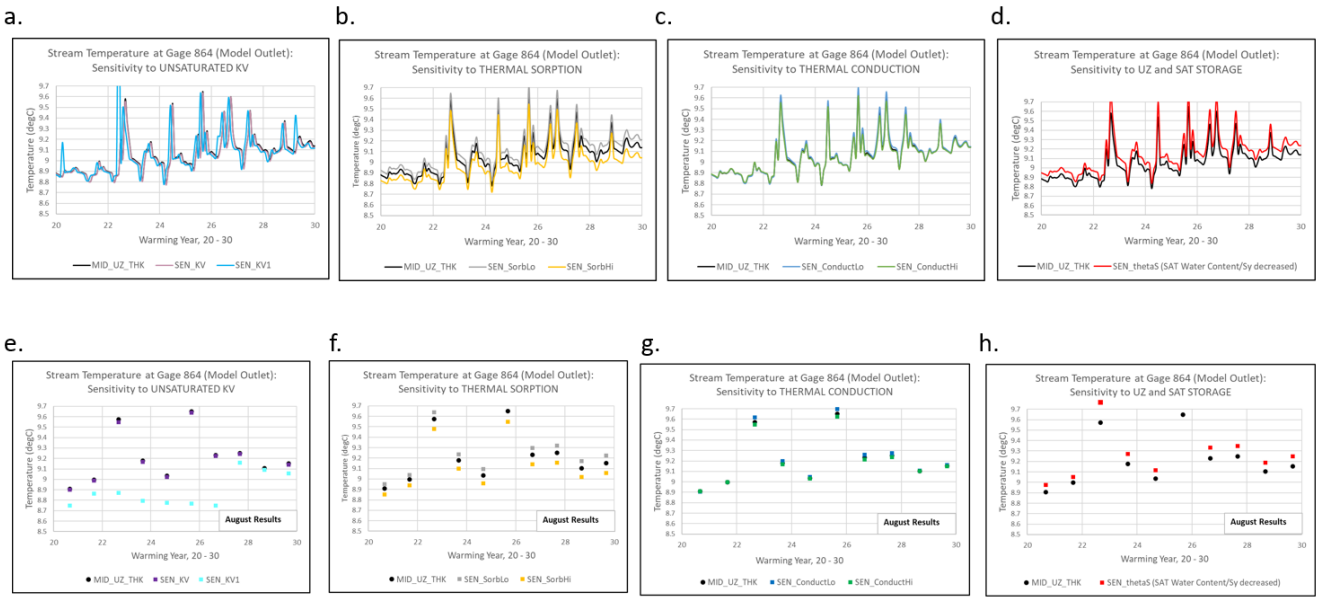

Figure S3-10. Sensitivity results for MID_UZ_THK model for stream temperatures at the model outlet gage during warming period, a) sensitivity to value of UZ vertical hydraulic conductivity, b) sensitivity to value of distribution coefficient for sorption, c) sensitivity to value of thermal conductivity for conduction, d) sensitivity to values of UZ and saturated storage parameters, e) sensitivity of August results to value of UZ vertical hydraulic conductivity, f) sensitivity of August results to value of distribution coefficient for sorption, g) sensitivity of August results to value of thermal conductivity for conduction, and h) sensitivity of August results to values of UZ and saturated storage parameters.

Expanded Discussion on Model Limitations

The proposed method for studying heat propagation in the subsurface neglects certain mechanisms and simplifies others, including:

- Root zone processes (i.e., evapotranspiration) are neglected and the infiltration rate is equated with the quantity of water that passes the zero-flux plane and enters the top of the unsaturated zone. Soil balance methods can be used to quantify this flux

through time [2]. More problematic are the transient temperature conditions to assign the infiltration flux. Our approach assumes the infiltration temperatures averaged over a monthly interval is equal to the atmospheric temperatures for the same interval, a convenient simplification unless there is reason to think that passage through the root zone resets the temperature up or down at the model time scale. The top of the unsaturated zone is represented by the 3-foot thick receptor layer. The thickness of the receptor layer is intended to correspond to the volume of the root zone; it can of course be adjusted and varied spatially to fit observed the root-zone thickness.

- The UZF package in MODFLOW implements simplifying assumptions associated with the kinematic wave approximation byneglecting capillarity and simulation of purely downward gravitational flow. The expectation is that this simplification is warranted at the watershed scale [3].
- The MODFLOW application yields three states for cells in any row/column stack–unsaturated, partly saturated (hosting the water table) and fully saturated. In the transfer of information from MODFLOW to the MT3D-USGS code, each cell is assigned a single volume-average water content. For the water-table case, this single water content is a mixed value reflecting the presence of both unsaturated and saturated conditions. In this study, sensitivity runs that refined the vertical discretization (and, therefore, edited the relative position of the water table) had little effect on temperature results, suggesting that this limitation on computational accuracy is minor.
- MT3D-USGS is a groundwater transport code; therefore, flux through the solid matrix is neglected. While there is no water movement through the solid phase, heat is, in fact, diffused through the matrix, and typically more rapidly than in the fluid phase. In our simulations a "bulk" diffusion term is applied to stand in for this transport mechanism. It simulates the propagation of the solid and fluid diffusive fronts as a joint movement, slower than purely solid thermal diffusion and faster than purely fluid thermal diffusion. The upward or downward thermal diffusion is expected to generally be a secondary phenomenon compared to convection (see the companion paper, Feinstein et al. (2022) [4], for a full transient analysis of its relative importance for the synthetic model), but there can be cases where, because the temperature gradient is unusually strong, the diffusive flux is dominant, and the "bulk" simplification possibly leads to structural error.
- The method under consideration is designed for temperate climate regions. It neglects processes such as mountain-front recharge and conditions such as deep water tables and long flow paths, characteristic of semi-arid regions, which give rise to thermal regimes at the watershed scale very different than those represented by the synthetic model.

The relevance and importance of these methodological limitations must be evaluated in the case of any proposed application. One objective of this paper was to show that neglect of the unsaturated zone in the analysis of subsurface heat propagation has a high cost, undermining the power of the model to simulate accurately the spread of the heat signal from the top of the unsaturated zone. It is necessary to weigh that cost against any bias introduced by simplifying assumptions (neglect of root zone, kinematic wave assumption, limited vertical resolution, bulk thermal conduction) made largely to make the transport calculations tractable.

A second group of limitations is not necessarily attached to the logic of the proposed methodology but arise from the way the synthetic model was implemented. Three are listed here:

- Time smoothing of drivers: that is, the use of a monthly climate forcing;
- Neglect of the thermal influence of storm runoff to streams: that is, the restriction of the simulation to baseflow conditions;

- Inadequate representation of components of the lake energy budget that influence lake temperature, such as neglect of phase changes (ice formation and melt), energy changes related to evaporation, and lake thermal stratification.

In principle, at least these limitations could be reduced by refining model input or adding functionality to MODFLOW packages.

An additional limitation arises from the solver technique applied to the synthetic model. The finite-difference method used to solve the transport equation is subject to mathematical errors in the form of numerical dispersion and artificial oscillation [5]. Substitution of the total-variation-diminishing (TVD) scheme for the advective component of transport within the finite-difference method is an option in MT3D for minimizing these errors [6]. However, all attempts to implement the TVD solver in the case of the MID_UZ_THK version of the base model led to solution instability. Although in areas of the model where the solution was stable the effect of numerical dispersion on the temperature results appeared small, it was not possible to make a full analysis of numerical dispersion by comparing TVD to finite-difference results in general.

Perhaps the most important qualification to be made regarding the construction of the synthetic model regards the form of the heat forcing function. The 50% average increase in the magnitude of the heat forcing function over 30 years (Figure S1-6), which is due less to the linear warming trend explicitly imposed than to the onset of variable monthly infiltration after spin-up, is not realistic. It should not be taken as representative of expected future climate conditions. However, it does serve heuristically to exercise the proposed method and clarify important relations controlling heat propagation.

References

1. Niswonger, R.G.; Prudic, D.E.; Regan, R.S. *Documentation of the Unsaturated-Zone Flow (UZF1) Package for Modeling Unsaturated Flow between the Land Surface and the Water Table with MODFLOW-2005*; 2328-7055; U.S. Geological Survey Scientific: Reston, VA, USA, 2006; p. 62. https://doi.org/10.3133/tm6A19
2. Westenbroek, S.M., Engott, J.A., Kelson, V.A., and Hunt, R.J. *SWB Version 2.0—A soil-water-balance code for estimating net infiltration and other water-budget components*: U.S. Geological Survey Techniques and Methods, book 6, chap. A59, 2018; p. 118 https://doi.org/10.3133/tm6A59.
3. Harter, T.; Hopmans, J.W. (Eds.) *Role of Vadose-Zone Flow Processes in Regional-Scale Hydrology: Review, Opportunities and Challenges*; Kluwer Academic Publishers: Wageningen, The Netherlands, 2004; pp. 179–208.
4. Feinstein, D.T.; Hunt, R.J.; Morway, E.D. Simulation of heat flow in a synthetic watershed: Lags and damping across multiple pathways under a climate-forcing scenario. *Water* **2022**, *14*, 2810. https://doi.org/10.3390/w14182810.
5. Zheng, C.; Bennett, G.D. *Applied Contaminant Transport Modeling*, 2nd ed.; John Wiley & Sons, Inc.: New York, NY, USA, 2002.
6. Zheng, C. 2010. MT3DMS V5.3: *A modular three-dimensional multispecies transport model for simulation of advection, dispersion, and chemical reactions of contaminants in groundwater systems: Supplemental user's guide* Accessed on August 25th, 2021. Available at <https://hydro.geo.ua.edu/mt3d/index.htm>